

Auger cascades in resonantly excited neon

MASTERARBEIT
zur Erlangung des akademischen Grades
„Master of Science“

eingereicht bei der
Physikalisch-Astronomischen Fakultät
der Friedrich-Schiller-Universität Jena

von Sebastian Stock
geboren am 21. März 1993 in Aalen

Jena, März 2017

Die in dieser Arbeit präsentierten Ergebnisse wurden ebenfalls in dem folgenden Artikel veröffentlicht:

S. Stock, R. Beerwerth, and S. Fritzsche. "Auger cascades in resonantly excited neon". To be submitted.

Erstgutachter: Prof. Dr. Stephan Fritzsche

Zweitgutachter: Priv.-Doz. Dr. Andrey Volotka

Abstract

The Auger cascades following the resonant $1s \rightarrow 3p$ and $1s \rightarrow 4p$ excitation of neutral neon are studied theoretically. In order to accurately predict Auger electron spectra, shake probabilities, ion yields, and the population of final states, the complete cascade of decays from neutral to doubly-ionized neon is simulated by means of extensive MCDF calculations. Experimentally known values for the energy levels of neutral, singly and doubly ionized neon are utilized in order to further improve the simulated spectra. The obtained results are compared to experimental findings. For the most part, quite good agreement between theory and experiment is found. However, for the lifetime widths of certain energy levels of Ne^+ , larger differences between the calculated values and the experiment are found. It is presumed that these discrepancies originate from the approximations that are utilized in the calculations of the Auger amplitudes.

Contents

1	Introduction	1
2	Overview of the Auger cascades	3
3	Theory	7
3.1	Calculation of Auger amplitudes	7
3.2	The MCDF method	8
3.3	Shake processes and the biorthonormal transformation	9
4	Calculations	11
4.1	Bound state wave function generation	11
4.2	Application of experimental energy levels	12
4.3	Analysis of the decay pathways	12
5	Results and discussion	17
5.1	Electron spectra	17
5.2	Shake probabilities	22
5.3	Ion yields	23
5.4	Lifetime widths of selected Ne ⁺ levels	23
6	Summary	27
7	Outlook	29
7.1	Computation of Auger amplitudes based on the full Hamiltonian	29
7.2	Computation of Auger amplitudes with separate orbital sets	30
7.3	Investigation of direct multiple Auger processes	30
7.4	Further development of the software used for the analysis of the cascade .	31
	Bibliography	33

1 Introduction

Inner-shell vacancies in light atoms decay predominantly via Auger decay, i.e., a radiationless process where an outer-shell electron is de-excited to fill the vacancy and another outer-shell electron is emitted from the atom and carries away the excess energy. Since the energy gained by filling an inner-shell vacancy can be sufficiently large to remove not only one but several outer-shell electrons, it is possible to achieve multiple ionization by a single photon (the one which creates the initial inner-shell hole). Such an Auger process where two electrons are emitted was first detected in 1965 by Carlson and Krause [1]. Since then, double Auger (DA) decays have been the subject of many experimental and theoretical studies.

In general, two competing DA mechanisms can be observed: *direct* DA and *cascade* DA. In the direct DA process, both electrons are emitted simultaneously and a continuous energy sharing between the two electrons can be observed [2, 3]. Since, from a theoretical viewpoint, the direct DA process arises from the interaction between three electrons, it only occurs in second- or higher-order perturbation theory. The cascade DA process on the other hand is a two-step process consisting of two subsequent single Auger decays: the first Auger decay leaves the atom in an autoionizing state, which then decays via a second Auger process.

Generally, both cascade and direct processes can contribute to the decay of an inner-shell vacancy. Especially when triple or higher ionization is achieved, combinations of direct multiple Auger and cascade Auger processes are generally involved [4]. Nevertheless, the direct DA can often be neglected if a cascade decay is possible and many studies, both experimental and theoretical, focus on the cascade process [5–9].

When the 1s electron of a near-neutral atom is excited to an otherwise empty np shell, cascade processes become particularly abundant. In this case, so-called *spectator* decays are possible and dominate over *participator* decays in filling the inner-shell vacancy. In the spectator process, the electron that is excited from the inner shell to a valence shell doesn't participate in the Auger decay that fills the inner-shell vacancy. Instead, it stays in

its excited state while an electron from a sub-valence shell fills the vacancy and another sub-valence electron is ejected. After the spectator decay, the ion often remains in a highly-excited (and therefore autoionizing) state and consequently undergoes a second Auger decay. In addition, so-called *shake processes* of the valence electron during the first Auger decay play an essential role. In a shake process, the sudden perturbation of the Auger decay leads to a jump of an electron to a higher or lower shell.

Over the past few decades, many aspects of the Auger decays of $1s \rightarrow np$ excited neon have been explored in great detail experimentally [5–7, 10–14]. However, detailed numerical simulations of these two-step decay cascades are still missing. In this thesis, the Auger cascades that follow resonant $1s \rightarrow 3p$ and $1s \rightarrow 4p$ photoexcitation of neutral neon are simulated. For this purpose, extensive MCDF calculations which include all likely decay paths are performed, with the goal of achieving a complete description of these cascades. The obtained electron spectra, ion yields, and shake probabilities are compared to experimental findings in order to evaluate whether this approach is appropriate for acquiring a complete and detailed view of these Auger cascades.

The results obtained in this study are also presented in a paper that is to be submitted soon. Consequently, large parts of the thesis overlap with the information presented in the paper. Some passages are quoted verbatim from an earlier version of the paper, in particular most of Chapter 3. A preliminary version of the paper is attached at the end of this thesis.

The thesis is structured as follows: In Chapter 2, the two-step Auger cascades following resonant excitation of the $1s^{-1}3p\ ^1P_1$ and $1s^{-1}4p\ ^1P_1$ levels of neon are introduced. Chapter 3 briefly explains the theory behind the calculations, i.e., the calculation of the Auger rates, the MCDF method, and the biorthonormal transformation. Chapter 4 first describes some aspects of the calculations in detail, namely the generation of the bound-state wave functions and the use of experimental energy levels in the calculations. Following this, the program that was developed in order to analyze the Auger cascades is briefly introduced. The results are discussed in Chapter 5. Parts of this chapter are intentionally kept short since the results are discussed in great detail in the attached paper. In Chapter 6, the findings are briefly summarized and conclusions are drawn. Finally, an overview of possible future steps is given in Chapter 7.

2 Overview of the Auger cascades

The starting point of the cascade is the resonant photoexcitation of the core-excited $1s^{-1}3p\ ^1P_1$ and $1s^{-1}4p\ ^1P_1$ levels of neutral neon, which is achieved for photon energies of 867.13 eV and 868.76 eV, respectively [15]. Compared to the $1s^{-1}np\ ^1P_1$ levels, an excitation of the neighboring $1s^{-1}np\ ^3P$ levels is suppressed by about three orders of magnitude, as was determined by calculating the appropriate Einstein coefficients with the REOS program of the RATIP [16] suite. Therefore, the population of the 3P levels can be neglected and only the Auger cascades of the initially excited $1s^{-1}np\ ^1P_1$ levels are considered in this study.

The Auger cascades that follow this resonant photoexcitation consist of two steps. In the first step, the core-excited atom emits a fast Auger electron and becomes a Ne^+ ion with a hole in either the 2s or 2p shell. For this first step of the cascade, all levels of Ne^+ that can be reached by either spectator *or* participator decays are included as possible final states of the Auger decays. Additionally, the initially excited 3p or 4p electron can undergo shake processes during the first Auger decay.

Usually, two electrons participate in an Auger decay, i.e., the de-excited and the emitted electron. In an Auger decay with a (single-electron) shake process, an additional third electron is displaced from its initial orbital towards a higher orbital (*shake-up*) or a lower one (*shake-down*). Shake processes mainly occur between subshells with the same orbital angular momentum, e.g., from the 3p to the 4p subshell. A shake process where the electron changes its orbital angular momentum is called *conjugate* shake process.

For the first step of the cascade, shake processes of the initially excited 3p or 4p spectator electron to any of the np subshells with $n = 3, \dots, 7$ are included in the computations. Shake-up processes to subshells with higher principal quantum number are negligible, as was determined by comparing results for $n = 6, 7$. According to a recent experimental study by Tamenori and Suzuki [14], *conjugate* shake processes where the 3p spectator electron jumps to the 3d subshell can also be observed, such as the $1s^{-1}3p \rightarrow 1s^22s^22p^4(^1D)3d$ transitions. To account for these transitions, shake processes to the 3d subshell are also

included in the computations. The possible decays in the first step of the Auger cascade can therefore be summarized as

$$\text{Ne } 1s^{-1}np \ ^1P_1 \rightarrow \text{Ne}^+ \left\{ \begin{array}{l} 1s^2 2s^2 2p^5 \\ 1s^2 2s^1 2p^6 \\ 1s^2 2s^2 2p^4 n'\ell \\ 1s^2 2s^1 2p^5 n'\ell \\ 1s^2 2s^0 2p^6 n'\ell \end{array} \right\} + e^- . \quad (2.1)$$

where $n'\ell \in \{3p, 3d, 4p, 5p, 6p, 7p\}$.

Some of the final states of the first step lie energetically above the Ne^{2+} ground state and are therefore autoionizing. These final states of the first step then become the initial states of the second step of the Auger cascade, in which Auger electrons with much lower energy are emitted. For this second step of the cascade, all final states that arise from the $2s^2 2p^4$ and $2s^1 2p^5$ configurations as well as several energetically allowed levels of the $2s^2 2p^3 n\ell$ configurations are included in the computations. This leads to the following decay channels in the second step of the cascade:

$$\begin{aligned} \text{Ne}^+ 1s^2 2s^2 2p^4 n\ell &\rightarrow \text{Ne}^{2+} 1s^2 2s^2 2p^4 + e^- , \\ \text{Ne}^+ 1s^2 2s^1 2p^5 n\ell &\rightarrow \text{Ne}^{2+} \left\{ \begin{array}{l} 1s^2 2s^2 2p^4 \\ 1s^2 2s^1 2p^5 \end{array} \right\} + e^- , \\ \text{Ne}^+ 1s^2 2s^0 2p^6 n\ell &\rightarrow \text{Ne}^{2+} \left\{ \begin{array}{l} 1s^2 2s^1 2p^5 \\ 1s^2 2s^2 2p^4 \\ 1s^2 2s^2 2p^3 n'\ell' \end{array} \right\} + e^- . \end{aligned} \quad (2.2)$$

Note that this includes an additional conjugate $2p \rightarrow 2s$ shake-down for the $2s^0 2p^6 n\ell \rightarrow 2s^2 2p^4$ and $2s^0 2p^6 n\ell \rightarrow 2s^2 p^3 n'\ell'$ Auger decays. Figure 2.1 shows the Ne^+ and Ne^{2+} energy levels that are involved in the considered Auger cascades. From this figure, it can be deduced that triple ionization is not possible if we consider only the configurations outlined in Eqs. (2.1) and (2.2), since the energetically highest Ne^{2+} level that can be reached by these transitions is well below the triple ionization threshold.

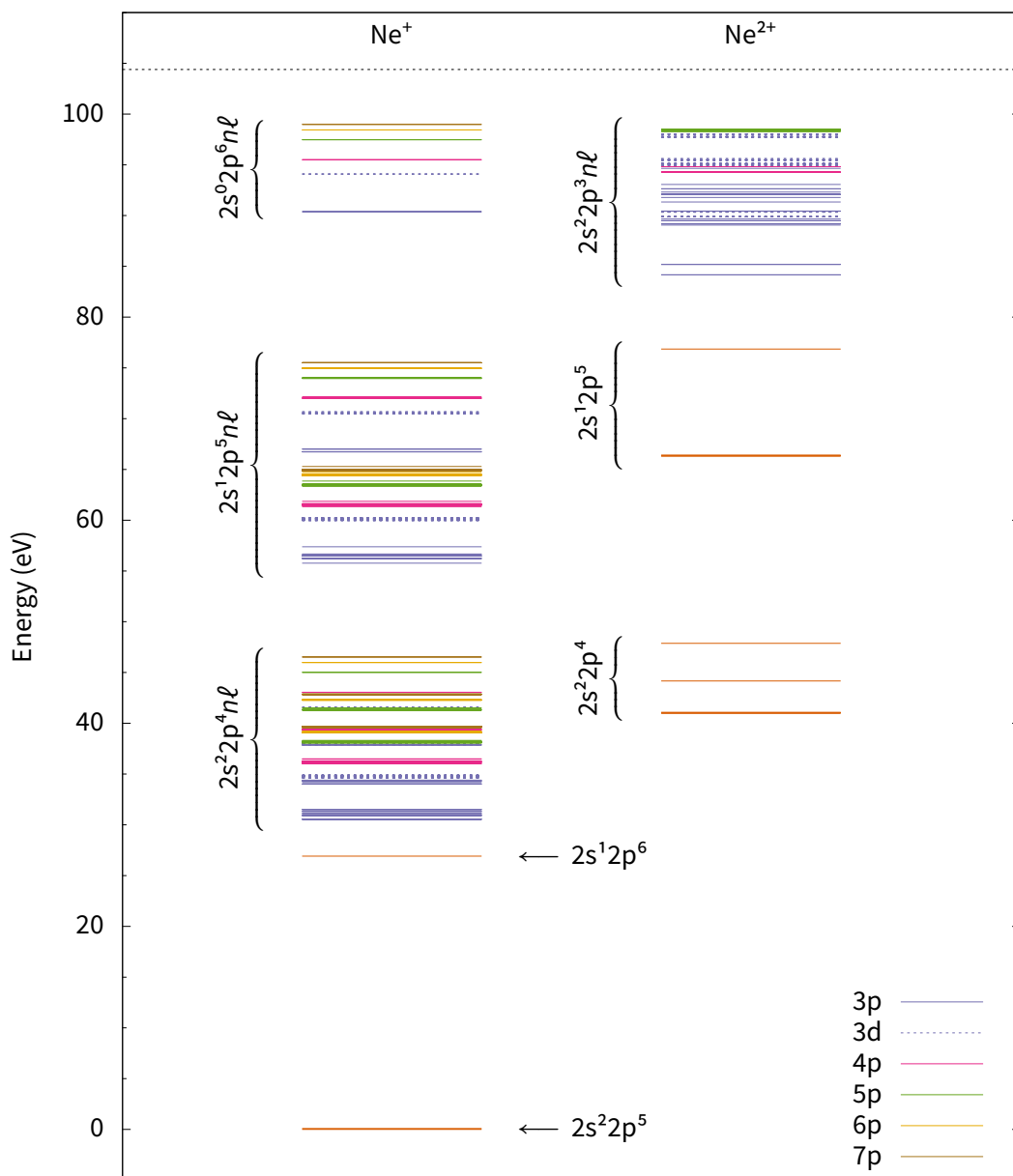


Figure 2.1. Energy levels of Ne^+ and Ne^{2+} relative to the Ne^+ $1s^2 2s^2 2p^5 \ ^2P_{3/2}$ ground level. Only the levels that are relevant for the cascade, as outlined in Eqs. (2.1) and (2.2), are shown. Experimental energies are employed whenever available and the energies of the remaining levels are interpolated based on the experimentally observed levels, cf. Section 4.2. The dashed line at 104.4 eV represents the triple ionization threshold.

3 Theory

In this chapter, the theoretical background of the calculations is briefly explained. Most of the content of this chapter is quoted verbatim from an early version of the paper that is attached at the end of the thesis.

The theory is based on the Dirac–Coulomb–Breit Hamiltonian

$$H = \sum_i h_D(\mathbf{r}_i) + V, \quad (3.1)$$

where h_D denotes the one-electron Dirac operator and V denotes the operator for the interelectronic interaction, i.e., the sum of the Coulomb and Breit interactions between each two electrons,

$$V = V_C + V_B = \sum_{i < j} \left(\frac{1}{r_{ij}} + b_{ij} \right). \quad (3.2)$$

3.1 Calculation of Auger amplitudes

Within the framework described in Ref. [17], which is based on the theory of resonance scattering, the Auger amplitude for the decay of an initial N -electron state $\Psi_i(P_i J_i M_i)$ with parity P_i , total angular momentum J_i , and projection of total angular momentum M_i into the final state $\Psi_f(P_f J_f M_f)$ with $N - 1$ electrons and respective parity, total angular momentum and projection thereof is given by

$$V_{i \rightarrow f, \kappa} = \langle \Psi_f, \epsilon \kappa; P_t J_t \parallel H - E \parallel \Psi_i; P_i J_i \rangle \delta_{P_i P_t} \delta_{J_i J_t} \delta_{M_i M_t}, \quad (3.3)$$

where $\epsilon \kappa$ denotes the partial wave of the ejected electron with energy ϵ and relativistic angular quantum number κ . The coupling of the final ionic state $\Psi_f(P_f J_f M_f)$ with the partial wave $\epsilon \kappa$ of the continuum electron yields a final state with parity P_t , total angular momentum J_t and projection of total angular momentum M_t .

Assuming that the wave functions for the initial and the final state are based on a common set of orthonormal orbitals, the contributions from the one-electron operators h_D and the energy E to the matrix element $V_{i \rightarrow f, \kappa}$ vanish, because two electrons are displaced in the Auger process. Only the interelectronic interaction operator V is non-vanishing, as it is composed of two-electron operators. Therefore, the AUGER component of the RATIP [16] package calculates the Auger amplitude as

$$V_{i \rightarrow f, \kappa} \approx \langle \Psi_f, \epsilon \kappa; P_t J_t \| V \| \Psi_i; P_i J_i \rangle \delta_{P_i P_t} \delta_{J_i J_t} \delta_{M_i M_t}. \quad (3.4)$$

where the partial waves $\epsilon \kappa$ of the continuum electron are generated as distorted waves within the potential of the corresponding final ionic state. From the amplitudes $V_{i \rightarrow f, \kappa}$, the respective Auger transition rate is then obtained as $\Gamma_{i \rightarrow f} = 2\pi \sum_{\kappa} |V_{i \rightarrow f, \kappa}|^2$, summing over all contributing partial waves.

3.2 The MCDF method

The bound state wave functions used for the computation of the Auger amplitudes are generated using the multiconfiguration Dirac–Fock (MCDF) method. Within the MCDF formalism, the atomic state function Ψ_{α} of an energy level α is constructed as a linear combination of so-called *configuration state functions* (CSF's) Φ with the well-defined parity P , total angular momentum J , and projection of total angular momentum M :

$$\Psi_{\alpha}(PJM) = \sum_{i=1}^{n_c} c_i(\alpha) \Phi(\gamma_i PJM), \quad (3.5)$$

where n_c denotes the number of CSF's and γ_i refers to the remaining quantum numbers that are required for specifying the CSF uniquely. The coefficients $\{c_i(\alpha)\}$ are the representation of the atomic state α in the given CSF basis. The N -electron CSF's in turn are constructed from a set of atomic orbitals, i.e., one-electron wave functions. A common set of orbitals is used for all CSF's. This set is constructed to be orthonormal, i.e., for two orbitals ϕ_i, ϕ_j from the same orbital set the relation $\langle \phi_i | \phi_j \rangle = \delta_{ij}$ holds.

Employing the programs of the GRASP [18] suite, the radial functions of the atomic orbitals are optimized self-consistently, and separately for the initial and final states of

the transitions, based on the Dirac–Coulomb Hamiltonian. Further relativistic effects due to the Breit interaction among the electrons, i.e., due to the magnetic and the retarded interaction, are incorporated by configuration interaction (CI). In a CI calculation, the eigenstates of an atomic system are computed by diagonalizing the Hamiltonian matrix $\mathbb{H} = \langle \Phi_i | H | \Phi_j \rangle$ to solve the eigenvalue problem $\mathbb{H}\mathbf{c} = E\mathbf{c}$, where E is the energy of the atomic eigenstate and the vector $\mathbf{c} = (c_1, \dots, c_{n_c})^T$ is the representation of the atomic eigenstate in the CSF basis $(\Phi_1, \dots, \Phi_{n_c})$.

3.3 Shake processes and the biorthonormal transformation

Since the initial and final bound state wave functions Ψ_i, Ψ_f differ in the number of electrons, their respective orbitals are shaped differently due to the orbital relaxation. The orbital sets $\{\phi_i\}, \{\phi'_i\}$ for the initial and the final states are therefore not *biorthonormal*, i.e., the relation $\langle \phi_i | \phi'_j \rangle = \delta_{ij}$ does not hold. This is particularly significant with regard to shake processes. From a simple viewpoint, shake processes arise from the overlap of different orbitals of the initial and final states, i.e., a shake-up from 3p to 4p requires that the 3p orbital of the initial state overlaps with the 4p orbital of the final state. In first approximation, the shake probability equals the modulus squared of this orbital overlap. In addition, mixing between different configurations will also lead to otherwise impossible channels that involve shake-up or -down transitions.

However, in the evaluation of the angular part of the Auger amplitudes, the AUGER program of the RATIP package assumes that the initial and final states are based on a common orthonormal set of orbitals. Therefore, to treat shake processes with the RATIP code, one has to account for the orbital overlap between initial and final states in a different way. In order to do that, the *biorthonormal transformation*, which has been described in detail by Olsen *et al.* [19] and is implemented in the GRASP suite, is applied to the orbital sets.

The biorthonormal transformation modifies two sets of orbital functions, $\{\phi_i\}, \{\phi'_i\} \mapsto \{\tilde{\phi}_i\}, \{\tilde{\phi}'_i\}$, such that the resulting orbitals fulfill $\langle \tilde{\phi}_i | \tilde{\phi}'_j \rangle = \delta_{ij}$. Transforming the orbitals naturally changes the CSF's that are used to represent the atomic states, $\Phi(\gamma_i P J M) \mapsto \tilde{\Phi}(\gamma_i P J M)$. In order to leave the atomic state functions invariant, the coefficients $c_i \mapsto \tilde{c}_i$

are transformed as well, so that

$$\sum_{i=1}^{n_c} c_i(\alpha) \Phi(\gamma_i P J M) = \sum_{i=1}^{n_c} \tilde{c}_i(\alpha) \tilde{\Phi}(\gamma_i P J M). \quad (3.6)$$

In this way, the original orbital overlap is accounted for via the mixing of different configurations. The biorthonormal transformation thus provides an elegant method to treat shake processes.

4 Calculations

In this study, the programs of the GRASP [18] suite were used to construct the bound-state wave functions and to perform the biorthonormal transformation for the orbitals of the initial and final states of each step of the cascades. Based on these bound-state wave functions, the Auger decay rates were calculated with the AUGER component of the RATIP [16] package. In order to analyze the decay pathways based on the computed Auger rates, a program which enables convenient access to electron spectra and other properties of the Auger cascade was developed.

In modeling the Auger cascade, the initial resonant photoexcitation as well as all subsequent Auger decays are treated as independent processes. In particular, a possible alignment of the atom due to the initial photoexcitation is not considered here, since it do not affect the angle-integrated electron spectra. *Direct* multiple Auger processes are also not considered in the present study, since they only occur in second- or higher-order perturbation theory.

4.1 Bound state wave function generation

Electron correlation effects are known to play a central role in the description of the atomic states. Therefore, additional atomic states that are not populated during the cascade process (i.e., Ne^{2+} states whose energies are higher than the highest considered Ne^+ state) are included in the calculations, because in many cases they mix with energetically low-lying states and therefore may affect the computation of the Auger rates. To model the relevant states of neutral, singly ionized, and doubly ionized neon, all CSF's of the following configurations are included in the calculations:

- Ne (24 CSF's): $1s^2s^22p^6nl$,
- Ne^+ (261 CSF's): $1s^22s^22p^5$, $1s^22s2p^6$, $1s^22s^22p^4nl$, $1s^22s2p^5nl$, $1s^22p^6nl$,

- Ne^{2+} (516 CSF's): $1s^2 2s^2 2p^4$, $1s^2 2s 2p^5$, $1s^2 2s^2 2p^3 n\ell$, $1s^2 2p^6$, $1s^2 2s 2p^4 n\ell$, $1s^2 2p^5 n\ell$,

where $n\ell \in \{3p, 3d, 4p, 5p, 6p, 7p\}$ in order to account for shake processes of the initially excited 3p or 4p electron as described in Chapter 2.

4.2 Application of experimental energy levels

The second step of the cascade includes a multitude of transitions with very low energies. In order to correctly reproduce these low-energy spectra, one has to distinguish energetically allowed transitions from energetically forbidden ones. The level energies obtained via *ab-initio* calculations, with a rather small basis set as employed here, are not accurate enough for these purposes. Relying solely on the calculated level energies produces some transitions that are energetically forbidden in reality, while at the same time excluding some other transitions that are actually observed in the experiment. Therefore, experimentally known level energies of Ne, Ne^+ , and Ne^{2+} are used in this study to better reproduce the energies of the emitted electrons. These experimental energies were obtained from several different sources:

- Energies of low-lying levels of Ne^+ (where available) and Ne^{2+} , as well as ionization energies are obtained from the NIST Atomic Spectra Database [20].
- Auger spectra from Refs. [6, 7, 14, 21, 22] are used for the determination of some additional Ne^+ energy levels that are not available from optical data.
- Values for the $1s^{-1}3p$ and $1s^{-1}4p$ excitation energies are obtained from Ref. [15].

However, there are energy levels for which there is no experimental data available. These level energies are therefore interpolated using the known energies of neighboring levels. The energy levels resulting from this procedure are shown in Figure 2.1 in Chapter 2.

4.3 Analysis of the decay pathways

The first step of the cascade contains 261, the second step 1512 transitions. In order to conveniently analyze the decay cascades that arise from these transitions, a program

was developed using the *Julia*¹ programming language. The program creates an internal representation of the Auger cascade based on Auger decay rates (which are read from the .sum files that are created by the AUGER program) and a distribution of initial states. From this, several different properties like electron spectra, ion yields, etc. can be easily obtained.

The program is organized in a module named AugerCascades. In this module, among other things, the composite data type AugerCascade defined, which is the representation of an Auger cascade in the code.

```
type AugerCascade
    states::Array{Array{State, 1}, 1}
    decays::Array{Array{AugerDecay, 1}, 1}
end
```

The AugerCascade object contains two fields:

- The field named `states` represents the atomic levels. It consists of an array which contains for each charge state an array of the included atomic levels. Such an atomic level is represented by an object of type `State`.
- The `decays` field which represents the Auger decays. It consists of an array which contains for each step of the cascade an array of `AugerDecay` objects, which represent the Auger transitions that occur in this step.

The `State` and `AugerDecay` objects are interlinked in order to form a graph-like structure: Each `AugerDecay` object has two fields `fromState` and `toState` which link to the respective initial and final states (i.e., the `State` objects) of the transition. Likewise, each `State` contains the fields `children` and `parents` which are arrays of links to the appropriate `AugerDecays`. (Note that an energy level can be populated via multiple different Auger decays, and can also decay via multiple different Auger decays.) Apart from these links, the `State` and `AugerDecay` objects include additional fields to store different properties,

¹ The Julia language is a high-level dynamic programming language that is designed with numerical and scientific computing in mind. As such, it attempts to combine the convenience of modern dynamic languages like Python with the performance of C or Fortran. Its syntax is influenced by MATLAB. It is a relatively young language (development started in 2009, the first version was published in 2012) and still developing rapidly. An introduction to the language is given in Ref. [23].

like the transition rate and energy for Auger transitions. In order to easier identify the energy levels, one can provide labels (typically an *LSJ*-coupled configuration state) to the State objects.

In order to create an AugerCascade object, the user has to specify an arbitrary number of .sum files created by the AUGER program. Each file must include the transitions of one step of the cascade, and they must be given in correct order. The easiest way to create an AugerCascade object is then to pass this list of file names to the constructor:

```
sumfiles = ["first_step.sum", "second_step.sum"]
mycascade = AugerCascade(sumfiles)
```

If the first file contains transitions from more than one initial state, the user gets prompted to specify the relative population of the initial states. For example, the Auger files that were created and analyzed in this study contain the transitions from all 24 Ne $1s^{-1}n\ell$ levels that are included in the MCDHF calculations. In order to analyze the decay of the $1s^{-1}3p\ ^1P_1$ level, which is the fourth level in the list, the dialog could look like this (user input in boldface):

```
There are 24 relevant initial states: 1-24
Populate single state? [Y/n] y
Enter state to populate: 4

Probabilities of initial states:
4:      1.0
```

Alternatively, the user can pass the initial population as an argument to the constructor in order to avoid the dialog.

Once an AugerCascade object is created, several functions can be applied to it to retrieve properties that are of interest. A few of them are introduced below to provide a little more insight into the capabilities of the program.

- The `ionields` function calculates the ion yields for the given Auger cascade. For example, for the cascade following the $1s^{-1}3p\ ^1P_1$ excitation, the resulting array would look like this: $[0.0, 0.744463, 0.255537]$. The elements of this array describe the probabilities for obtaining a Ne, Ne^+ , and Ne^{2+} atom/ion after the decay cascade, respectively (cf. Table 5.3).

- The `electronSpectrum` function returns a table that contains the energies and relative intensities of each transition in the cascade. Instead of including all transitions it is also possible to obtain just the transitions for a specific step of the cascade. While the table that is returned by `electronSpectrum` contains only the energies and intensities of the transitions, there exists a function `verboseElectronSpectrum` which, in addition, also includes the initial and final states for each transition (including their assigned labels, if available) as well as their natural linewidths.

In order to make use of the tables created by these functions, the `printtable` and `plotspectrum` functions are provided:

- The `printtable` function writes tabular data to the standard output. It is not limited to the tables obtained via the `electronSpectrum` function but can be used on arbitrary two-dimensional arrays. At that, the output it produces is well-suited for the presentation of tabular data. For example, in columns that include numerical data, the values are automatically aligned at the decimal point and can be rounded if desired.
- The `plotspectrum` function creates plot data (i.e., x and y values) from the tables created by the `electronSpectrum` function. This data can then be displayed using one of the plotting packages for the Julia language, or written into a `.csv` file for use with other plotting software.

If no further arguments are passed to the function, every transition is plotted as a Gaussian with a constant FWHM of 100 eV. Alternatively, the line profile can be specified by passing a Gaussian and/or a Lorentzian width to the function. Optionally, the individual (calculated) linewidths of each transition can be used for the Lorentzian widths. In this case, the user can still specify an additional Gaussian width to simulate Doppler and/or instrumental broadening.

- Furthermore, several functions to obtain properties of individual transitions or energy levels are provided, for example the `linewidth` function. This function can be used on both `AugerDecays` and on `States`, returning the natural linewidth for an Auger transition or the lifetime width for an atomic level.

5 Results and discussion

In this chapter, the results of modeling the complete two-step Auger cascade following the resonant photoexcitation of the $1s^{-1}3p\ ^1P_1$ and $1s^{-1}4p\ ^1P_1$ levels of neutral neon are presented. With the exception of the discussion of the lifetime widths in Section 5.4, the discussion in this chapter is kept short, as the results are discussed in detail in the attached paper.

5.1 Electron spectra

The first step of the cascade comprises the transitions from the initially excited $1s^{-1}np\ ^1P_1$ level to all 261 levels of Ne^+ that are considered above in Eq. 2.1. In this step, fast Auger electrons with energies between 746 eV and 848 eV are emitted. The simulated Auger electron spectra are shown in Figure 5.1. For the sake of simplicity, every transition is plotted as a Gaussian with a constant FWHM of 100 meV. The peaks that are numbered in the spectra are listed together with their intensities in the paper that is attached at the end of the thesis.

The dominant peaks of the first-step spectra lie in the energy range between 799 eV and 817 eV and belong to the transitions to the fine-structure levels of the $2s^22p^4n\ell$ configurations. This part of the first-step spectra has been explored extensively in the past. For comparison, the simulated spectra for this energy range are shown together with experimental spectra obtained by Tamenori and Suzuki [14] in Figure 5.2. In Table 5.1, the calculated intensities for the transitions from the initially excited $Ne\ 1s^{-1}3p\ ^1P_1$ level to the $2s^22p^43p$ levels of Ne^+ are compared with experimental values from Kivimäki *et al.* [12].

The dashed vertical lines in the spectra in Fig. 5.1 signify the double ionization threshold. Transitions with an Auger electron energy higher than this threshold populate levels that lie energetically below the Ne^{2+} ground level and therefore are not ionized further. On the

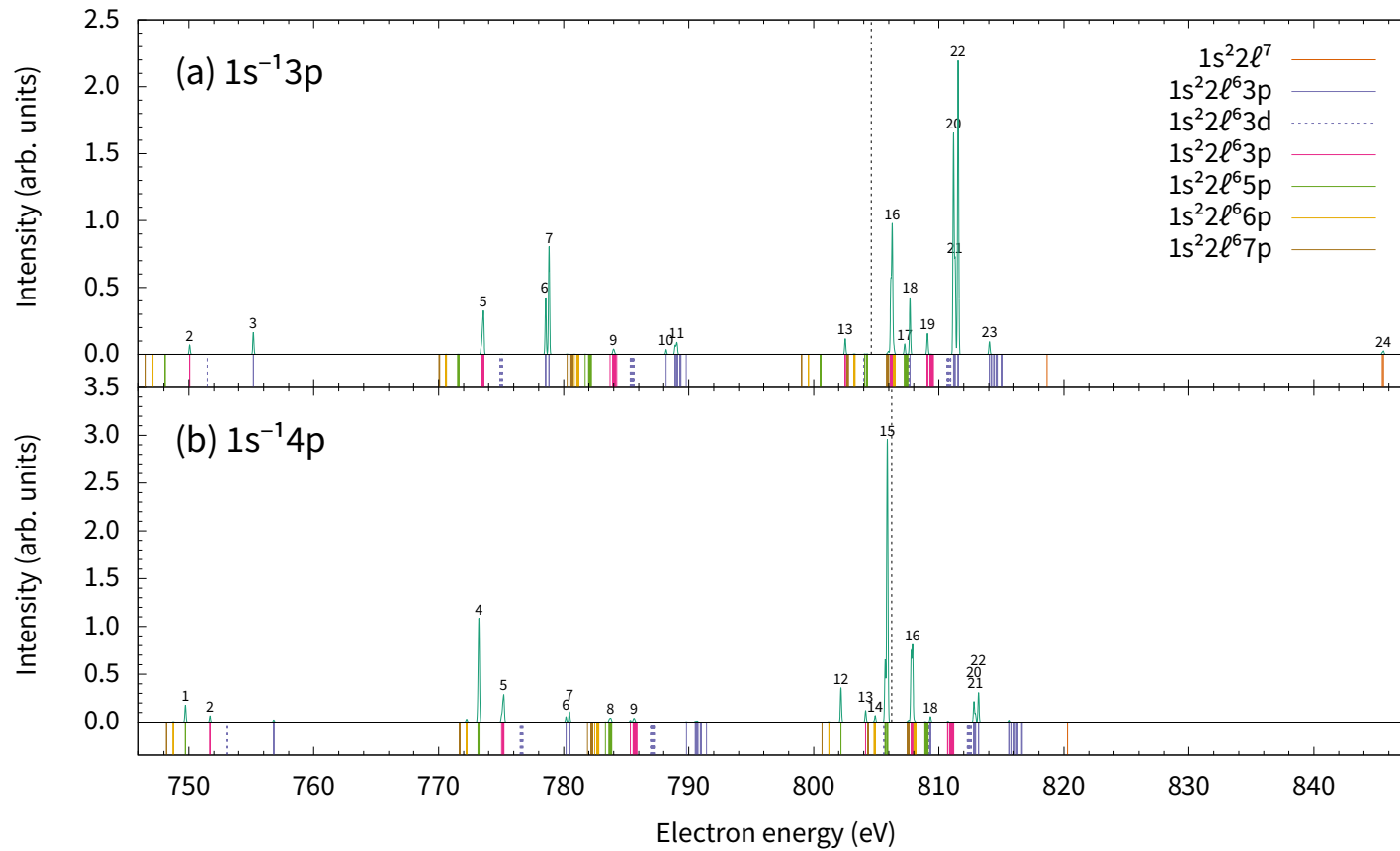


Figure 5.1. Simulated Auger electron spectra for the first step of the cascade decay of the core-excited (a) $1s^{-1}3p\ ^1P_1$ and (b) $1s^{-1}4p\ ^1P_1$ levels of neon. Every transition is plotted as a Gaussian with a FWHM of 100 meV. The intensities of the numbered peaks are listed in the attached paper. The vertical lines below the plots indicate all possible transitions in the first step of the cascade, where the colors correspond to different final-state configurations, cf. the legend. The dashed lines at (a) 804.6 eV and (b) 806.2 eV signify the double ionization threshold: transitions located to the left of these lines lead to Ne^+ levels which are autoionizing and thus participate in the second step of the cascade.

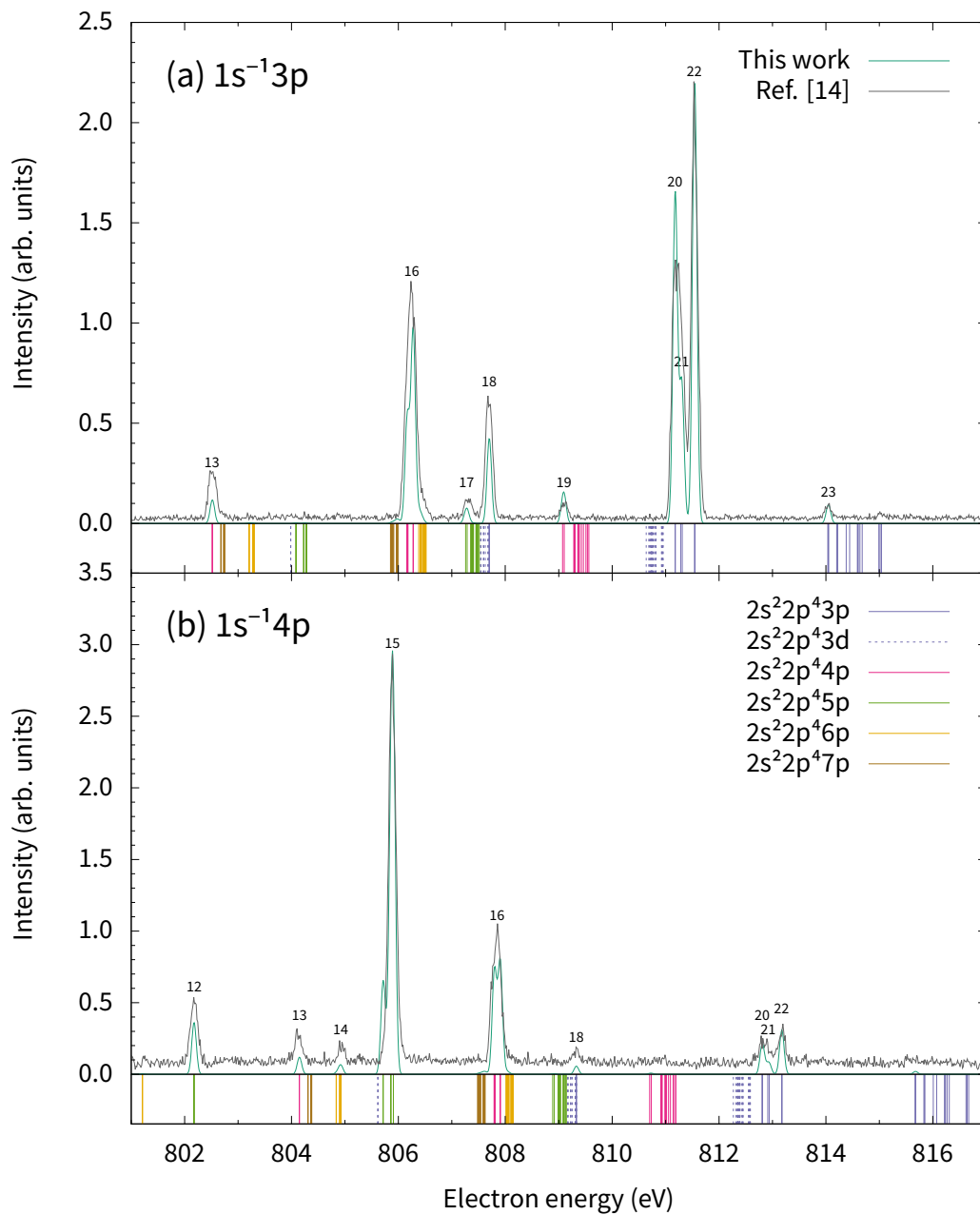


Figure 5.2. Comparison of an enlarged part of Figure 5.1 (green curves) with experimental spectra (grey curves) obtained by Tamenori and Suzuki [14]. The part of the spectra displayed here contains the transitions from the initially excited Ne $1s^{-1}np\ ^1P_1$ level to the $2s^2 2p^4 n\ell$ levels of Ne⁺.

Table 5.1. Relative intensities of the transitions from the core-excited Ne $1s^{-1}3p^1P_1$ level to different multiplet of the Ne⁺ $2s^22p^43p$ configuration. Experimental intensities obtained by Kivimäki *et al.* [12] are given for comparison. The numbers in the first column refer to the labels of the peaks in Figure 5.1(a). The intensities are given in relation to that of the largest peak, i.e., Peak 22. Since the intensities are normalized differently in the experimental study, they are scaled appropriately in order to enable comparison.

№	Final state(s)	E_k	Intensity	
			This work	Ref. [12]
18	$2s^22p^4(^1S)3p^2P$	807.7	0.192	0.321
20	$2s^22p^4(^1D)3p^2D$	811.2	0.744	0.725
21	$2s^22p^4(^1D)3p^2P$	811.3	0.333	0.373
22	$2s^22p^4(^1D)3p^2F$	811.5	1.0	1.0
23	$2s^22p^4(^3P)3p^2P$	814.0	0.043	0.027

other hand, transitions that emit an electron with a kinetic energy below this threshold populate levels that lie energetically above the Ne²⁺ ground level. These levels then decay to Ne²⁺ via one of the second-step transitions listed in Eq. (2.2).

The second step of the cascade comprises all energetically allowed transitions between the fine-structure levels of those configurations of Ne⁺ and Ne²⁺ that are considered above in Eq. 2.2, which amounts to 1512 transitions in total. In this step, Auger electrons with energies between 0 and 59 eV are emitted. The simulated Auger electron spectra are shown in Figure 5.3. Again, every transition is plotted as a Gaussian with a constant FWHM of 100 meV. The peaks that are numbered in the spectra are listed together with their intensities in the paper that is attached at the end of the thesis.

The second-step spectrum can be roughly divided into three parts which feature different types of transitions:

- The low-energy part (0–8 eV) is dominated by *multiplet-changing Auger transitions*. In these transitions, the energy required for the emission of the Auger electron is not provided by a change of the configuration of the electronic core but instead by a change of its multiplet coupling. Consequently, these transitions emit electrons of very low energy since the energy gained by changing the multiplet coupling of the electronic core is usually small. In addition to the multiplet-changing transitions, most of the $2s^02p^6n\ell \rightarrow 2s^22p^3n'\ell'$ transitions lie also in this energy range. However,

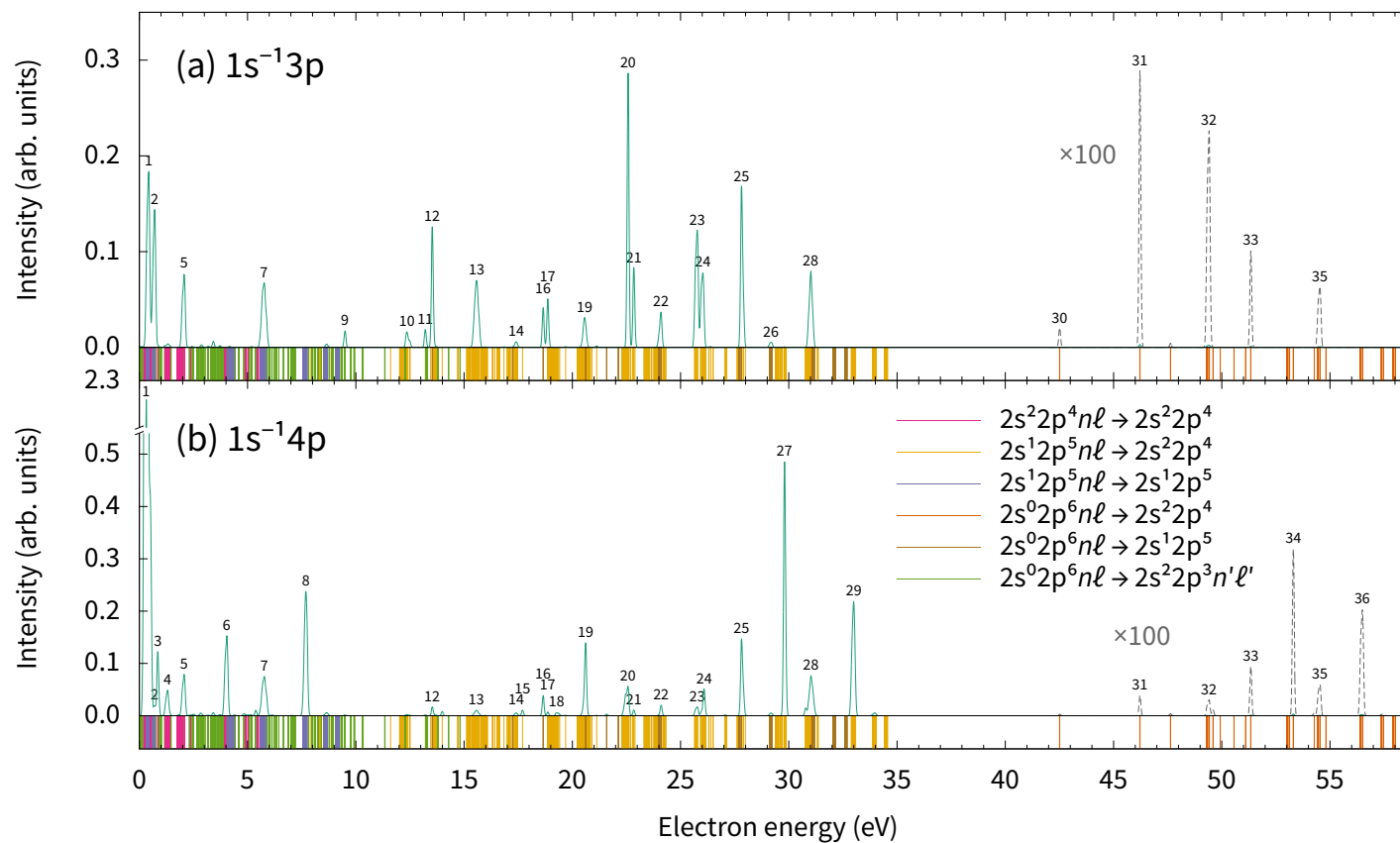


Figure 5.3. The same as Fig. 5.1, but for the second-step Auger decays. The intensities of the numbered peaks are listed in the attached paper. The colors of the vertical lines below the plots correspond to different initial and final configurations, cf. the legend. For electron energies higher than 42 eV, the graphs are enhanced by a factor of 100 to make the $2s^0 2p^6 nl \rightarrow 2s^2 2p^4$ transitions visible.

Table 5.2. Calculated probabilities for shake processes of the 3p or 4p valence electron to another subshell during the first step of the cascade. Experimental values obtained by Tamemori and Suzuki [14] are given for comparison.

Final subshell	1s ⁻¹ 3p excitation		1s ⁻¹ 4p excitation	
	This work	Ref. [14]	This work	Ref. [14]
3p	0.72	} 0.69	0.096	} 0.08
3d	2.9 × 10 ⁻⁴		5.6 × 10 ⁻⁵	
4p	0.26	0.31	0.24	0.26
5p	0.0099	< 0.01	0.64	0.64
6p	0.0085	< 0.01	0.015	0.02
7p	0.0036	< 0.01	0.0033	< 0.01

their intensities are generally negligible. This is expected, since these transitions include a conjugate shake-down 2p → 2s and are therefore highly suppressed compared to normal Auger decays. They have not been observed experimentally.

- The energy range 8–35 eV contains the 2s¹2p⁵nℓ → 2s²2p⁴ and 2s⁰2p⁶nℓ → 2s¹2p⁵ transitions. This part of the spectrum has been explored experimentally before, see the attached paper for a comparison of the calculated intensities for the 1s⁻¹3p excitation with experimental data by Yoshida *et al.* [6].
- The energy range 42–59 eV contains the 2s⁰2p⁶nℓ → 2s²2p⁴ transitions. Like the 2s⁰2p⁶nℓ → 2s²2p³nℓ transitions, they include a conjugate shake-down 2p → 2s and therefore play a minor role. They have not been observed experimentally. In Figure 5.3, they are enhanced by a factor of 100 in order to make them visible.

5.2 Shake probabilities

As can be seen from Figure 5.2, the probabilities of shake processes during the first step of the cascade can be predicted quite accurately. The shake probabilities for the initially excited 3p or 4p electron are shown in Table 5.2. Experimental data from Ref. [14] is given for comparison and shows good agreement. The data indicates that conjugate shake processes to the 3d subshell are highly suppressed and can be neglected.

Table 5.3. Ion yields after resonant excitation to the Ne $1s^{-1}3p\ ^1P_1$ and $1s^{-1}4p\ ^1P_1$ levels. The calculated values are shown together with experimental values obtained by Morgan, Sagurton, and Bartlett [24].

Charge state	$1s^{-1}3p$ excitation		$1s^{-1}4p$ excitation	
	This work	Ref. [24]	This work	Ref. [24]
Ne ⁺	0.74	0.65 ± 0.02	0.24	0.24 ± 0.03
Ne ²⁺	0.26	0.31 ± 0.02	0.76	0.71 ± 0.04
Ne ³⁺	—	0.03 ± 0.01	—	0.04 ± 0.01
Ne ⁴⁺	—	0.002	—	0.002

5.3 Ion yields

The calculated ion yields are shown in Table 5.3 together with experimental values obtained by Morgan, Sagurton, and Bartlett [24]. The values obtained in this study show reasonably good agreement with the experimental findings. While triply and even quadruply charged neon ions are observed in the experiment, they are not included in this study since they are a result of higher order processes such as direct double and triple Auger decays or shake processes due to more complex correlation patterns.

5.4 Lifetime widths of selected Ne⁺ levels

Another way of estimating the accuracy of the calculations is the comparison of calculated lifetime widths with experimental data. Since the lifetime width Γ of an energy level is directly proportional to its total decay rate, this allows a direct evaluation of the calculated Auger rates.

The lifetime widths of selected Ne⁺ multiplets have been measured by Ueda *et al.* [22] and De Fanis *et al.* [25]. In Table 5.4, the calculated lifetime widths for these multiplets are shown together with the experimental values. The comparison shows that some of the lifetime widths, and therefore the corresponding Auger rates, are significantly overestimated. In particular, the widths of the $2s^12p^5(^1P)np\ ^2S_{1/2}$ ($n = 3, 4$) levels exceed the experimental values by factors of 8 and 6, respectively. Some other widths are overestimated by factors of up to 4, while still others are reproduced quite well. The large deviations for

Table 5.4. Lifetime widths for selected levels of Ne^+ . The computed values are shown together with experimental widths obtained by Ueda *et al.* [22] and De Fanis *et al.* [25]. Results from a theoretical study of the $2s^1 2p^5(^3,^1\text{P})3p^2 S_{1/2}$ levels by Sinanis, Aspromallis, and Nicolaides [26] are also shown for comparison.

Level(s)	Lifetime width (meV)		
	Theory		
	This work	Ref. [26]	
$2s^1 2p^5(^3\text{P})3p^2 \text{D}$	65		80 ± 10 [22]
$2s^1 2p^5(^3\text{P})3p^2 \text{P}$	71		19 ± 5 [22]
$2s^1 2p^5(^3\text{P})3p^2 S_{1/2}$	293	122	120 ± 10 [22]
$2s^1 2p^5(^3\text{P})4p^2 S_{1/2}$	121		30 ± 15 [25]
$2s^1 2p^5(^1\text{P})3p^2 S_{1/2}$	4289	510	530 ± 50 [22]
$2s^1 2p^5(^1\text{P})3p^2 \text{D}$	17		34 ± 5 [22]
$2s^1 2p^5(^1\text{P})3p^2 \text{P}$	47		42 ± 5 [22]
$2s^1 2p^5(^1\text{P})4p^2 S_{1/2}$	803		135 ± 20 [25]
$2s^0 2p^6 3p^2 \text{P}$	82		80 ± 5 [25]
$2s^0 2p^6 4p^2 \text{P}$	36		20 ± 5 [25]

the $2s^1 2p^5(^3,^1\text{P})3p^2 S_{1/2}$ levels are especially surprising, since an older theoretical study by Sinanis, Aspromallis, and Nicolaides [26], which calculates the decay widths of these levels based on multiconfiguration Hartree–Fock calculations, produces results that agree very well with the experimental findings.

The $2s^1 2p^5(^1\text{P})3p^2 S_{1/2}$ and $2s^1 2p^5(^1\text{P})4p^2 S_{1/2}$ levels, which are overestimated the most, decay predominantly via multiplet-changing transitions to the $2s^1 2p^5\ ^3\text{P}$ levels of Ne^{2+} . In our calculations, more than 98% of the total decay rate of these levels is due to multiplet-changing transitions. This is in contrast to the $2s^1 2p^5(^1\text{P})3p^2 \text{P}$ and ^2D levels, which decay mostly via normal Auger decay to the $\text{Ne}^{2+} 2s^2 2p^4$ ground configuration. Therefore, it is suspected that the overestimated Auger rates are (at least partially) due to the calculation of the Auger rates for multiplet-changing transitions.

It seems natural that the approximative calculation of the Auger amplitudes by the AUGER program is not appropriate for multiplet-changing Auger transitions: The characterising feature of these transitions is that only one electron is displaced in the process, while

the remaining electrons only change their multiplet coupling. In this case, the one-electron operators h_D , which are neglected in the calculation of the Auger amplitude by the AUGER program (cf. Section 3.1), do not necessarily vanish even when biorthonormal orbital sets are used.

6 Summary

In the present thesis, the two-step Auger cascades following the resonant photoexcitation of the $1s^{-1}3p\ ^1P_1$ and $1s^{-1}4p\ ^1P_1$ core-excited levels in neon were explored theoretically. For this purpose, extensive MCDF calculations were performed in order to incorporate all likely intermediate and final states as well as all major correlations into the description. The aim of this work was to assess as to what extent such a complete simulation of Auger cascades is feasible and produces results that compare well to experimental findings.

The Auger rates of all considered transitions were calculated with the AUGER component of the RATIP package based on bound-state wave functions that were created with the programs of the GRASP suite. The biorthonormal transformation was applied to the initial and final states of each transition in order to account for shake processes, which arise from the relaxation of the atomic orbitals during the Auger decay. In order to analyze the resulting Auger cascades, a program was developed that enables the user to obtain different properties of these Auger cascades, such as Auger electron spectra, ion yields, and the population of different levels.

Whenever available, experimental level energies for the considered Ne, Ne⁺, and Ne²⁺ levels were used instead of the energies from the *ab initio* calculations. This was necessary in order to accurately simulate the low-energy part of the spectra and to predict ion yields that are in good agreement with the experiment. While the accuracy of the *ab initio* energy levels might be further improved by systematically increasing the CSF basis to include more correlation effects, it is doubtful whether this would suffice to correctly reproduce the low-energy transitions that are observed in the experiment.

For the most part, the Auger electron spectra that were simulated in this study agree well with experimental findings. However, there are a few exceptions where there is a larger discrepancy between the theoretical results presented here and the experiment.

The calculated shake probabilities for the first step of the cascade agree well with experimental data. Shake processes of the initially excited *np* electron to a different orbital

$n'p$ occur often and are important for a complete description of the cascade. On the other hand, conjugate shake processes to the 3d orbital are found to be suppressed by several orders of magnitude. The calculated ion yields also agree well with experimental findings if one takes into account that direct multiple Auger decays, which may lead to charge states higher than Ne^{2+} , are not included in this study.

Although the analysis of the simulated Auger electron spectra shows good agreement between theory and experiment, the lifetime widths for some of the $2s^1 2p^5 3p$ and $2s^1 2p^5 4p$ levels, are significantly overestimated. Since these discrepancies are especially large for levels which decay dominantly via multiplet-changing transitions, it is suspected that they are due to approximations in the calculation of the Auger amplitude which are not applicable for multiplet-changing transitions.

In conclusion, the approach to model the complete cascades of Auger decays from the core-excited Ne $1s^{-1}3p \ ^1P_1$ and $1s^{-1}4p \ ^1P_1$ levels via large-scale MCDF calculations can be considered successful. By including all possible participator and spectator decays as well as shake processes due to a simple model, most features of these Auger cascades, that are well-known from experimental studies, can be reproduced with good agreement if experimental level energies are employed.

7 Outlook

This chapter outlines topics of possible future work that builds upon the findings from this thesis. Some of the shortcomings of this study are pointed out and possible steps to address them are proposed. These future steps mostly amount to modification or extension of the RATIP code.

7.1 Computation of Auger amplitudes based on the full Hamiltonian

Analysis of the lifetime widths for some of the $2s^1 2p^5 3p$ and $2s^1 2p^5 4p$ levels of Ne^+ (cf. Section 5.4) reveals large deviations between some of the calculated values and experimental data, while an older theoretical study is able to accurately reproduce the experimental decay widths. Since those levels which decay dominantly via multiplet-changing transitions are the most affected by this, it is suspected that the approximative calculation of the Auger amplitudes by the AUGER program is not appropriate for these transitions.

This stands to reason, since only one electron is displaced during a multiplet-changing transition, and thus the one-electron operators h_D , which are neglected in the calculation of the Auger amplitude by the AUGER program, do not necessarily vanish. Furthermore, since the continuum orbitals for the emitted electron are generated to be orthogonal to the bound-state wave function of the *final* ion [16], there might be an overlap between the initial bound-state orbital and the final continuum orbital of the emitted electron. In this case, the total energy E might also contribute to the Auger amplitude and the complete $H - E$ term would have to be considered.

The effect of the one-electron operators h_D and the total energy E on the Auger amplitude should therefore be investigated in the context of multiplet-changing transitions. If a significant effect is found, the option to calculate the Auger amplitude with the full $H - E$ term could be incorporated in the AUGER program.

7.2 Computation of Auger amplitudes with separate orbital sets

The AUGER component of the RATIP package assumes a common set of orthonormal orbitals in the evaluation of the angular part of the Auger amplitude [16]. In this study, the biorthonormal transformation is applied to the orbital sets of the initial and final states in order to take the orbital relaxation into account. After the transformation, the two separately optimized orbital sets are biorthonormal, but the resulting orbitals (naturally) still differ from each other. This might affect the evaluation of the (angular part of) the Auger amplitude with the AUGER program. One could investigate how strongly this affects the result of the calculations, and, if necessary, revise the evaluation of the Auger amplitudes in the AUGER program.

7.3 Investigation of direct multiple Auger processes

Direct multiple Auger processes are not included in our study, as they only occur in higher-order perturbation theory and are expected to contribute to a lesser degree. However, various experimental and theoretical studies suggest that the branching ratios of direct double Auger processes can be of the same order of magnitude as those of cascade decays and can even exceed them [4, 27–30]. According to a study by Hayaishi *et al.* [27], the contributions of direct double Auger processes to the decay of the $1s^{-1}3p$ and $1s^{-1}4p$ core-excited levels of neon are significant, making up 9% of the total decays for the $1s^{-1}3p$ excitation and 32% for the $1s^{-1}4p$ excitation. However, given the method used in the study, these values should be considered estimates. Considering this, it would be interesting to get a detailed view of the double Auger processes that occur in the decay of these core-excited levels.

Usually, theoretical studies consider the direct double Auger processes in terms of the *shake-off* and *knock-out* mechanisms [31, 32]. In the shake-off mechanism, the orbital relaxation due to the (primary) Auger decay leads to a jump of the secondary electron to a continuum state. In this way it is similar to a shake-up or shake-down process. In the knock-out mechanism, the electron emitted in the primary Auger decay subsequently knocks out a second electron in an inelastic scattering process that corresponds to electron-

impact ionization. From a computational viewpoint, both of these approximations of the higher-order direct double Auger process are based on the single Auger decay rate and therefore allow a comparatively easy treatment of direct double Auger processes by computational means. Taking both mechanisms into account yields results that are in good agreement with experimental findings.

Since there is a sizeable interest in direct double Auger processes, one could consider to extend the RATIP code in order to treat these processes via the shake-off and knock-out mechanisms. This is a challenging task that would involve major additions to the codebase. First of all, the code would have to be extended in order to allow a second electron in the continuum. The computation formulae for both shake-off and knock-out mechanism include a sum over intermediate states with one electron in the continuum as well as an integration over continuum states, the latter to account for the continuous energy sharing between the electrons. Furthermore, for the knock-out mechanism, the collision strength for the electron-impact ionization of the intermediate ionic state by the primary Auger electron has to be calculated.

7.4 Further development of the software used for the analysis of the cascade

In its current state, the program provides various functions to retrieve different properties (e.g., electron spectra and ion yields) that are of interest when studying Auger cascades. It also provides relatively convenient access to the underlying data. However, there are still several parts that should be improved if the program is considered for further use.

For example, the output of plots and tables could be further simplified by providing functions that automate the export to different formats. Tables for example could be written to standard output or saved as .csv files or L^AT_EX documents, the latter of which currently still requires some work from the user. In addition, the program could benefit significantly from the incorporation of more appropriate data structures for tabular data. Right now, tables are simply represented by two-dimensional arrays that can hold elements of any type. A more database-like representation could make it easier to access and manipulate

the data and would also make the code a lot clearer. Even though this is a rather technical issue, it could also simplify the handling of tables for the user.

Apart from these modifications, the program could be extended to enable a more convenient analysis of shake processes. In the current state of the program, the calculation of shake probabilities is still left to the user. In order to improve on this, an appropriate way of representing shake models within the program would have to be developed. Based on this, the probabilities of shake processes that are due to different (user-defined) shake models could be calculated. Furthermore, the program could then also be extended to assist the calculations for such Auger cascades, by generating configuration lists for possible decay paths from a given initial electron configuration and according to shake models of varying complexity.

Bibliography

- [1] T. A. Carlson and M. O. Krause. “Experimental Evidence for Double Electron Emission in an Auger Process”. *Physical Review Letters* **14** (1965), 390–392. DOI: [10.1103/PhysRevLett.14.390](https://doi.org/10.1103/PhysRevLett.14.390).
- [2] J. Viefhaus, S. Cvejanović, B. Langer, T. Lischke, G. Prümper, D. Rolles, A. V. Golovin, A. N. Grum-Grzhimailo, N. M. Kabachnik, and U. Becker. “Energy and Angular Distributions of Electrons Emitted by Direct Double Auger Decay”. *Physical Review Letters* **92** (2004), 083001. DOI: [10.1103/PhysRevLett.92.083001](https://doi.org/10.1103/PhysRevLett.92.083001).
- [3] J. Viefhaus, A. N. Grum-Grzhimailo, N. M. Kabachnik, and U. Becker. “Electron–electron coincidence study of double Auger processes in atoms”. *Journal of Electron Spectroscopy and Related Phenomena* **141** (2004), 121–126. DOI: [10.1016/j.elspec.2004.06.013](https://doi.org/10.1016/j.elspec.2004.06.013).
- [4] Y. Hikosaka, T. Kaneyasu, P. Lablanquie, F. Penent, E. Shigemasa, and K. Ito. “Multiple Auger decay of the neon 1s-core-hole state studied by multielectron coincidence spectroscopy”. *Physical Review A* **92** (2015), 033413. DOI: [10.1103/PhysRevA.92.033413](https://doi.org/10.1103/PhysRevA.92.033413).
- [5] H. Yoshida, K. Ueda, N. M. Kabachnik, Y. Shimizu, Y. Senba, Y. Tamenori, H. Ohashi, I. Koyano, I. H. Suzuki, R. Hentges, J. Viefhaus, and U. Becker. “Angle-resolved study of the Auger electron cascades following the 1s → 3p photoexcitation of Ne”. *Journal of Physics B: Atomic, Molecular and Optical Physics* **33** (2000), 4343–4352. DOI: [10.1088/0953-4075/33/20/311](https://doi.org/10.1088/0953-4075/33/20/311).
- [6] H. Yoshida, J. Sasaki, Y. Kawabe, Y. Senba, A. De Fanis, M. Oura, S. Fritzsche, I. P. Sazhina, N. M. Kabachnik, and K. Ueda. “Study of second-step Auger transitions in Auger cascades following 1s → 3p photoexcitation in Ne”. *Journal of Physics B: Atomic, Molecular and Optical Physics* **38** (2005), 465–486. DOI: [10.1088/0953-4075/38/5/001](https://doi.org/10.1088/0953-4075/38/5/001).

- [7] M. Kitajima, H. Yoshida, A. De Fanis, G. Prümper, U. Hergenhahn, E. Kukk, T. Tanaka, K. Nakagawa, H. Tanaka, S. Fritzsche, I. P. Sazhina, N. M. Kabachnik, and K. Ueda. “A study of inner-valence Auger transitions in Ne^+ induced by the resonant Auger decay of photoexcited $\text{Ne } 1s^{-1}np$ states”. *Journal of Physics B: Atomic, Molecular and Optical Physics* **39** (2006), 1299–1322. DOI: [10.1088/0953-4075/39/6/004](https://doi.org/10.1088/0953-4075/39/6/004).
- [8] J. Andersson, R. Beerwerth, P. Linusson, J. H. D. Eland, V. Zhaunerchyk, S. Fritzsche, and R. Feifel. “Triple ionization of atomic Cd involving $4p^{-1}$ and $4s^{-1}$ inner-shell holes”. *Physical Review A* **92** (2015), 023414. DOI: [10.1103/PhysRevA.92.023414](https://doi.org/10.1103/PhysRevA.92.023414).
- [9] S. Schippers, R. Beerwerth, L. Abrok, S. Bari, T. Buhr, M. Martins, S. Ricz, J. Viefhaus, S. Fritzsche, and A. Müller. “Prominent role of multielectron processes in K -shell double and triple photodetachment of oxygen anions”. *Physical Review A* **94** (2016), 041401(R). DOI: [10.1103/PhysRevA.94.041401](https://doi.org/10.1103/PhysRevA.94.041401).
- [10] H. Aksela, S. Aksela, J. Tulkki, T. Åberg, G. M. Bancroft, and K. H. Tan. “Auger emission from the resonantly excited $1s^1 2s^2 2p^6 3p$ state of Ne”. *Physical Review A* **39** (1989), 3401–3405. DOI: [10.1103/PhysRevA.39.3401](https://doi.org/10.1103/PhysRevA.39.3401).
- [11] Y. Shimizu, H. Yoshida, K. Okada, Y. Muramatsu, N. Saito, H. Ohashi, Y. Tamenori, S. Fritzsche, N. M. Kabachnik, H. Tanaka, and K. Ueda. “High resolution angle-resolved measurements of Auger emission from the photo-excited $1s^{-1}3p$ state of Ne”. *Journal of Physics B: Atomic, Molecular and Optical Physics* **33** (2000), L685–L689. DOI: [10.1088/0953-4075/33/20/105](https://doi.org/10.1088/0953-4075/33/20/105).
- [12] A. Kivimäki, S. Heinäsmäki, M. Jurvansuu, S. Alitalo, E. Nömmiste, H. Aksela, and S. Aksela. “Auger decay at the $1s^{-1}np$ ($n = 3-5$) resonances of Ne”. *Journal of Electron Spectroscopy and Related Phenomena* **114-116** (2001), 49–53. DOI: [10.1016/S0368-2048\(00\)00259-0](https://doi.org/10.1016/S0368-2048(00)00259-0).
- [13] F. Da Pieve, L. Avaldi, R. Camilloni, M. Coreno, G. Turri, A. Ruocco, S. Fritzsche, N. M. Kabachnik, and G. Stefani. “Study of electronic correlations in the Auger cascade decay from $\text{Ne}^* 1s^{-1}3p$ ”. *Journal of Physics B: Atomic, Molecular and Optical Physics* **38** (2005), 3619–3630. DOI: [10.1088/0953-4075/38/19/014](https://doi.org/10.1088/0953-4075/38/19/014).

- [14] Y. Tamenori and I. H. Suzuki. “Multiplet exchange Auger transitions following resonant Auger decays in Ne 1s photoexcitation”. *Journal of Physics B: Atomic, Molecular and Optical Physics* **47** (2014), 145001. DOI: [10.1088/0953-4075/47/14/145001](https://doi.org/10.1088/0953-4075/47/14/145001).
- [15] M. Kato, Y. Morishita, M. Oura, H. Yamaoka, Y. Tamenori, K. Okada, T. Matsudo, T. Gejo, I. H. Suzuki, and N. Saito. “Absolute Photoionization Cross Section with an Ultra-high Energy Resolution for Ne in the Region of 1s Rydberg States”. *AIP Conference Proceedings* **879** (2007), 1121–1124. DOI: [10.1063/1.2436260](https://doi.org/10.1063/1.2436260).
- [16] S. Fritzsche. “The RATIP program for relativistic calculations of atomic transition, ionization and recombination properties”. *Computer Physics Communications* **183** (2012), 1525–1559. DOI: [10.1016/j.cpc.2012.02.016](https://doi.org/10.1016/j.cpc.2012.02.016).
- [17] T. Åberg and G. Howat. “Theory of the Auger Effect”. In: *Corpuscles and Radiation in Matter I*. Ed. by S. Flügge and W. Mehlhorn. Vol. 31. Encyclopedia of Physics. Berlin and Heidelberg: Springer-Verlag, 1982, pp. 469–619.
- [18] P. Jönsson, X. He, C. Froese Fischer, and I. P. Grant. “The grasp2K relativistic atomic structure package”. *Computer Physics Communications* **177** (2007), 597–622. DOI: [10.1016/j.cpc.2007.06.002](https://doi.org/10.1016/j.cpc.2007.06.002).
- [19] J. Olsen, M. R. Godefroid, P. Jönsson, P. Å. Malmqvist, and C. Froese Fischer. “Transition probability calculations for atoms using nonorthogonal orbitals”. *Physical Review E* **52** (1995), 4499–4508. DOI: [10.1103/PhysRevE.52.4499](https://doi.org/10.1103/PhysRevE.52.4499).
- [20] A. Kramida, Yu. Ralchenko, J. Reader, and NIST ASD Team. *NIST Atomic Spectra Database*. Version 5.4. 2016. URL: <http://physics.nist.gov/asd> (visited on Dec. 12, 2016).
- [21] A. De Fanis, G. Prümper, U. Hergenhahn, E. Kukk, T. Tanaka, M. Kitajima, H. Tanaka, S. Fritzsche, N. M. Kabachnik, and K. Ueda. “Investigation of valence intermultiplet Auger transitions in Ne following 1s photoelectron recapture”. *Journal of Physics B: Atomic, Molecular and Optical Physics* **38** (2005), 2229–2243. DOI: [10.1088/0953-4075/38/13/015](https://doi.org/10.1088/0953-4075/38/13/015).

- [22] K. Ueda, M. Kitajima, A. De Fanis, Y. Tamenori, H. Yamaoka, H. Shindo, T. Furuta, T. Tanaka, H. Tanaka, H. Yoshida, R. Sankari, S. Aksela, S. Fritzsche, and N. M. Kabachnik. “Doppler-Free Resonant Raman Auger Spectroscopy of $\text{Ne}^+ 2s2p^5 3p$ Excited States”. *Physical Review Letters* **90** (2003), 153005. DOI: [10.1103/PhysRevLett.90.153005](https://doi.org/10.1103/PhysRevLett.90.153005).
- [23] J. Bezanson, A. Edelman, S. Karpinski, and V. B. Shah. *Julia: A Fresh Approach to Numerical Computing*. Version 4. 2015. arXiv: [1411.1607v4](https://arxiv.org/abs/1411.1607v4) [cs.MS]. (Visited on Jan. 4, 2017).
- [24] D. V. Morgan, M. Sagurton, and R. J. Bartlett. “Single-photon multiple ionization of neon in the K -edge region”. *Physical Review A* **55** (1997), 1113–1118. DOI: [10.1103/PhysRevA.55.1113](https://doi.org/10.1103/PhysRevA.55.1113).
- [25] A. De Fanis, Y. Tamenori, M. Kitajima, H. Tanaka, and K. Ueda. “Doppler-free resonant Raman Auger spectroscopy study on atoms and molecules”. *Journal of Electron Spectroscopy and Related Phenomena* **137–140** (2004), 271–276. DOI: [10.1016/j.elspec.2004.02.062](https://doi.org/10.1016/j.elspec.2004.02.062).
- [26] Ch. Sinanis, G. Aspromallis, and C. A. Nicolaides. “Electron correlation in the Auger spectra of the $\text{Ne}^+ K 2s2p^5 ({}^3, {}^1P^o) 3p {}^2S$ satellites”. *Journal of Physics B: Atomic, Molecular and Optical Physics* **28** (1995), L423–L428. DOI: [10.1088/0953-4075/28/13/003](https://doi.org/10.1088/0953-4075/28/13/003).
- [27] T. Hayaishi, E. Murakami, Y. Morioka, E. Shigemasa, A. Yagishita, and F. Koike. “Decay channels following $1s$ photoexcitation of neon”. *Journal of Physics B: Atomic, Molecular and Optical Physics* **28** (1995), 1411–1420.
- [28] J. Zeng, P. Liu, W. Xiang, and J. Yuan. “Level-to-level and total probability for Auger decay including direct double processes of $\text{Ar } 2p^{-1}$ hole states”. *Physical Review A* **87** (2013), 033419. DOI: [10.1103/PhysRevA.87.033419](https://doi.org/10.1103/PhysRevA.87.033419).
- [29] J. L. Zeng, P. F. Liu, W. J. Xiang, and J. M. Yuan. “Complete Auger decay pathways of $\text{Kr } 3d^{-1}$ hole levels including direct double processes”. *Journal of Physics B: Atomic, Molecular and Optical Physics* **46** (2013), 215002. DOI: [10.1088/0953-4075/46/21/215002](https://doi.org/10.1088/0953-4075/46/21/215002).

-
- [30] F. Zhou, Y. Ma, and Y. Qu. “Single, double, and triple Auger decay probabilities of $C^+(1s2s^22p^2\ ^2D, \ ^2P)$ resonances”. *Physical Review A* **93** (2016), 060501(R). DOI: [10.1103/PhysRevA.93.060501](https://doi.org/10.1103/PhysRevA.93.060501).
- [31] M. Ya. Amusia, I. S. Lee, and V. A. Kilin. “Double Auger decay in atoms: Probability and angular distribution”. *Physical Review A* **45** (1992), 4576–4587. DOI: [10.1103/PhysRevA.45.4576](https://doi.org/10.1103/PhysRevA.45.4576).
- [32] T. Schneider, P. L. Chocian, and J.-M. Rost. “Separation and Identification of Dominant Mechanisms in Double Photoionization”. *Physical Review Letters* **89** (2002), 073002. DOI: [10.1103/PhysRevLett.89.073002](https://doi.org/10.1103/PhysRevLett.89.073002).

Erklärung

Hiermit erkläre ich an Eides statt, die vorliegende Arbeit selbstständig und nur unter Verwendung der angegebenen Quellen und Hilfsmittel verfasst zu haben. Die Stellen, die anderen Werken dem Wortlaut oder dem Sinn nach entnommen wurden, sind in jedem einzelnen Fall durch die Angabe der Herkunft kenntlich gemacht. Alle Grafiken wurden von mir selbst erstellt.

Die Arbeit wurde in dieser oder ähnlicher Form bisher bei keiner anderen Institution eingereicht.

Seitens des Verfassers bestehen keine Einwände, die vorliegende Arbeit für die öffentliche Nutzung in der Thüringer Universitäts- und Landesbibliothek zur Verfügung zu stellen.

Jena, 19. März 2017

.....

Sebastian Stock

Paper

Auger cascades in resonantly excited neon

S. Stock,^{1,2,*} R. Beerwerth,^{1,2} and S. Fritzsche^{1,2}

¹*Helmholtz Institute Jena, Fröbelstieg 3, 07743 Jena, Germany*

²*Theoretisch-Physikalisches Institut, Friedrich-Schiller-Universität Jena, 07743 Jena, Germany*

(Dated: March 19, 2017)

The Auger cascades following the resonant $1s \rightarrow np$ ($n = 3, 4$) excitation of neutral neon are studied theoretically. In contrast to previous investigations, we here model the complete cascade from the initially core-excited $1s^{-1}3p \ ^1P_1$ and $1s^{-1}4p \ ^1P_1$ levels of Ne up to the doubly-ionized Ne^{2+} ions. Extensive multiconfiguration Dirac-Fock (MCDF) calculations are carried out, combined with a proper cascades model, to incorporate as many decay branches as possible, including all major single-electron shake-up and shake-down processes. We simulate the electron spectra and predict shake probabilities, ion yields, as well as the relative population of the intermediate and final states. Experimentally known level energies for neutral, singly- and doubly-ionized neon are utilized whenever possible in order to improve the predictions. Most features from experiment can be reproduced with quite good agreement if a sufficiently large basis is taken into account. These simulations therefore demonstrate not only the required computational effort, but also that it is nowadays possible to predict whole Auger spectra of decay cascades, a central feature for further exploring electron coincidence maps as obtained at synchrotrons and free-electron lasers.

I. INTRODUCTION

Auger electron spectroscopy has been found a versatile tool for studying the electronic structure of atoms and molecules. In particular, the autoionization of inner-shell excited or ionized noble gases has been investigated extensively in the past decades [1–9]. Apart from plasma and astrophysics, such autoionization studies are of fundamental interest to better understand the dynamics of atoms and molecules in intense radiation fields.

Double and even multiple autoionization of atoms is often possible if an inner-shell vacancy is created. Such a double Auger (DA) process was first detected in 1965 [1]. Generally, two different and competing DA mechanisms are distinguished, namely the (so-called) *direct* and *cascade* DA. While the direct DA process is a high-order process in which both electrons share the (transition) energy and are ejected simultaneously [10], a subsequent electron emission occurs in the cascade DA process. In good approximation, the cascade DA decay can be described by a two-step process in which the first step still leads to an autoionizing state that can decay by further electron emission. Usually, a DA process is a combination of both, direct and cascade processes [9]. For medium and heavy atoms, moreover, inner-shell excitations often result even in triple or multiple ionization [11]. Recently, even a *direct triple* Auger decay was observed for the first time [12]. To describe such direct processes, the shake-off and knock-out mechanisms have been proposed [13, 14].

Auger cascades have been studied extensively, both experimentally and theoretically [15–19]. In particular, if a $1s$ electron of a nearly-neutral atom is excited to an otherwise empty np shell, such cascades frequently proceed via *spectator* processes, in which the excited

valence-shell electron itself does not participate in the autoionization in the first step. Therefore, the ions are often left in an autoionizing state and then undergo a second Auger decay. For such electron emission cascades, shake processes are known to play an essential role [2–4, 6, 8] and require special care in any theoretical description.

Although the Auger electron spectra of $1s \rightarrow 3p$ and $1s \rightarrow 4p$ excited neon have been explored experimentally [3, 5, 6, 8, 15–17, 20], a detailed numerical simulation of the overall two-step Auger cascades is still missing to the present. In this work, we therefore investigate the single and double autoionization of neon atoms with an initial K-shell hole, following the resonant $1s \rightarrow 3p$ and $1s \rightarrow 4p$ photoexcitation. For these cascades, we performed extensive MCDF computations in which all major single-electron shake-up and shake-down processes are incorporated systematically into the calculation of the Auger rates for all possible decay paths. As far as available, we compare our results to experiments and find good agreement for our simulated spectra as well as for shake probabilities and ion yields.

Our paper is structured as follows: In section II, we first introduce in detail the two Auger cascades following the inner-shell excitation of the $1s^{-1}3p \ ^1P_1$ and $1s^{-1}4p \ ^1P_1$ levels of neon, respectively, which are the focus of this work. Here, we also briefly outline the MCDF method as well as the biorthonormal transformation that is used in evaluating the Auger amplitudes and rates. Section III then describes further details about the generation of the systematically enlarged wave functions, and how we make use of experimental energies to further improve the simulated spectra. Our results are discussed in section IV which is subdivided into two parts, one which addresses the first step of the cascade as well as the shake probabilities and ion yields, and another part in which the second step of the cascade and the population of the final states are discussed. Finally, a short summary of our findings is given in Section V.

* sebastian.stock@uni-jena.de

II. THEORY

A. Auger cascades after inner-shell excitation

In neutral neon, the resonant photoexcitation of a 1s electron leads to the core-excited $1s^{-1}3p\ ^1P_1$ level at the (well-known) photon energy 867.13 eV, or to the $1s^{-1}4p\ ^1P_1$ level at 868.76 eV, respectively [21]. In comparison, the photoexcitation of the neighboring $1s^{-1}np\ ^3P$ levels from the 1S_0 ground state is typically suppressed by a factor of about 10^{-3} . Therefore, we here restrict ourselves to the Auger cascades of the initially excited $1s^{-1}np\ ^1P_1$ levels.

There are two major steps in the cascade decay of $1s^{-1}np\ ^1P_1$ core-excited neon atoms. In a first step, these atoms emit a fast Auger electron within ≈ 3 fs and become Ne^+ ions with a hole in either the 2s or 2p shell. For this first step of the cascade, we shall take into account all those levels that can be reached by spectator *or* participator decays as well as by single-electron shake-up or shake-down processes of the initially excited 3p or 4p electron. In addition to the two electrons that *normally* participate in any Auger decay, i.e., the de-excited and the emitted electron, in single-electron shake processes, a third electron is displaced from its shell into a higher subshell (*shake-up*) or a lower one (*shake-down*). If, moreover, the (shaken) electron changes its orbital angular momentum, we refer to this as a *conjugate* shake process. In the first step of the cascades, we here include all shake processes of the initially excited 3p or 4p spectator electron to any of the np subshells with $n = 3, \dots, 7$, as well as conjugate shake transitions to the 3d subshell. Therefore, the first step of the Auger cascades above can be summarized as

$$\text{Ne } 1s^{-1}np\ ^1P_1 \rightarrow \text{Ne}^+ \left\{ \begin{array}{l} 1s^2 2s^2 2p^5 \\ 1s^2 2s^1 2p^6 \\ 1s^2 2s^2 2p^4 n'l \\ 1s^2 2s^1 2p^5 n'l \\ 1s^2 2s^0 2p^6 n'l \end{array} \right\} + e^-. \quad (1)$$

Some of the final states on the right-hand side of step (1) are still autoionizing since they lie above the double ionization threshold. These final states of the first step then become the *initial* states of the second step of the Auger cascade, in which electrons with much lower energy are emitted. For this second step of the cascade, we include all final states that arise from the $2s^2 2p^4$ and $2s^1 2p^5$ configurations, as well as several energetically allowed

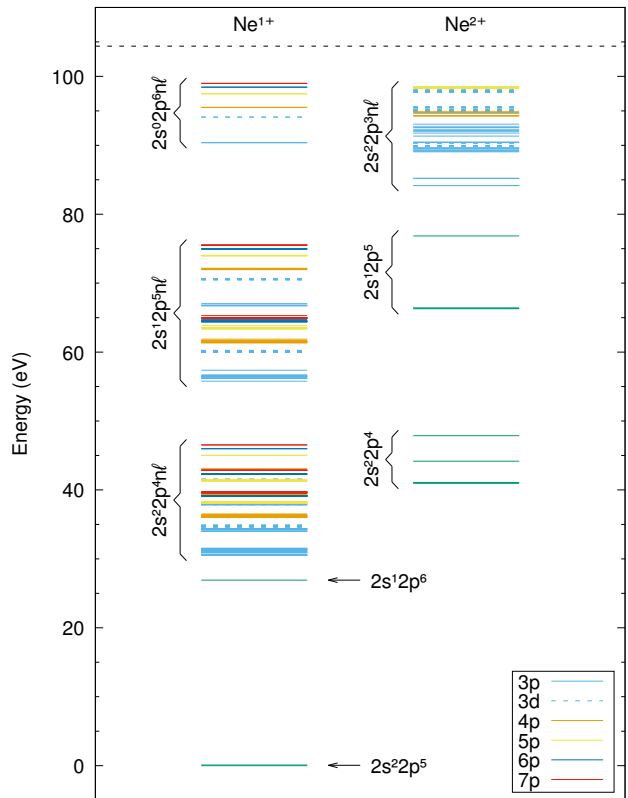


FIG. 1. Energy levels of Ne^+ and Ne^{2+} ions relative to the $1s^2 2s^2 2p^5\ ^2P_{3/2}$ ground level of Ne^+ . Only the levels that are relevant for the cascade as outlined in Eqs. (1) and (2) are shown. Here, we employed experimental level energies whenever available and interpolated the energies of the remaining levels based on experimentally observed levels, cf. section III B. The dashed line at 104.4 eV represents the triple ionization threshold.

levels from the $2s^2 2p^3 nl$ configurations:

$$\begin{aligned} \text{Ne}^+ 1s^2 2s^2 2p^4 nl &\rightarrow \text{Ne}^{2+} 1s^2 2s^2 2p^4 + e^-, \\ \text{Ne}^+ 1s^2 2s^1 2p^5 nl &\rightarrow \text{Ne}^{2+} \left\{ \begin{array}{l} 1s^2 2s^2 2p^4 \\ 1s^2 2s^1 2p^5 \end{array} \right\} + e^-, \\ \text{Ne}^+ 1s^2 2s^0 2p^6 nl &\rightarrow \text{Ne}^{2+} \left\{ \begin{array}{l} 1s^2 2s^1 2p^5 \\ 1s^2 2s^2 2p^4 \\ 1s^2 2s^2 2p^3 n'l \end{array} \right\} + e^-. \end{aligned} \quad (2)$$

In addition to the shake transitions of the nl valence electron, as mentioned above, we here included also the conjugate $2p \rightarrow 2s$ shake-down displacements in order to account for the energetically allowed Auger transitions between the fine-structure levels of the $2s^0 2p^6 nl \rightarrow 2s^2 2p^4$ and $2s^1 2p^5 nl \rightarrow 2s^2 2p^3 n'l'$ configurations, respectively.

Fig. 1 displays the energy levels of the Ne^+ and Ne^{2+} ions that are involved in the considered Auger cascades. As seen from this figure, triple ionization is not possible

if we consider only the configurations outlined in Eqs. (1) and (2), since the energetically highest of the considered Ne^+ levels is well below the triple ionization threshold.

In contrast to previous computations, in which only a few selected decay paths were considered (cf. e.g. Refs. [5, 16]), we here model all the possible decay branches that are outlined in Eqs. (1) and (2) in order to find the dominant decay paths and to account for all major correlation contributions from the various electronic configurations.

We do not include the $1s^2 2s^0 2p^6 n\ell \rightarrow 1s^2 2s^1 2p^4 n'\ell' + e^-$ Auger transitions since, based on our calculated *ab-initio* energy levels, the $2s^1 2p^4 n'\ell'$ levels are situated slightly above the $2s^0 2p^6 n\ell$ levels. However, the difference is below the uncertainty of the calculations, so we cannot rule out the existence of these transitions in the observed spectra.

B. Calculation of Auger transition rates

Our calculations are based on the Dirac–Coulomb–Breit Hamiltonian

$$H = \sum_i h_{\text{D}}(\mathbf{r}_i) + V, \quad (3)$$

where h_{D} denotes the one-electron Dirac operator and V the interelectronic interaction operator, i.e., the sum of the Coulomb and Breit interactions between each pair of electrons,

$$V = V_{\text{C}} + V_{\text{B}} = \sum_{i < j} \left(\frac{1}{r_{ij}} + b_{ij} \right). \quad (4)$$

Within the framework of Ref. [22], based on the theory of resonant scattering, the Auger amplitude for the decay of an initial N -electron state $\Psi_i(P_i J_i M_i)$ with parity P_i , total angular momentum J_i , and projection of total angular momentum M_i into the $(N-1)$ -electron final state $\Psi_f(P_f J_f M_f)$, with the respective quantum numbers P_f, J_f, M_f , is given by

$$V_{i \rightarrow f, \kappa} = \langle \Psi_f, \epsilon \kappa; P_t J_t || H - E || \Psi_i; P_i J_i \rangle \times \delta_{P_i P_t} \delta_{J_i J_t} \delta_{M_i M_t}, \quad (5)$$

where $\epsilon \kappa$ designates the partial wave of the ejected electron with kinetic energy ϵ and relativistic angular momentum quantum number κ . The coupling of the final ionic state $\Psi_f(P_f J_f M_f)$ with the partial wave $\epsilon \kappa$ of the continuum electron yields a final scattering state with total parity P_t and angular momentum J_t, M_t .

If the wave functions of the initial and the final states are constructed from a common set of orthonormal orbitals, neither the one-electron operators h_{D} nor the total energy E can contribute to the matrix element $V_{i \rightarrow f, \kappa}$ within a single-configuration approximation. This Auger amplitude then purely results from the two-electron interaction operator V . In the AUGER component of the

RATIP [23] package, the Auger amplitude is therefore simply calculated as

$$V_{i \rightarrow f, \kappa} \approx \langle \Psi_f, \epsilon \kappa; P_t J_t || V || \Psi_i; P_i J_i \rangle \delta_{P_i P_t} \delta_{M_i M_t} \delta_{J_i J_t}, \quad (6)$$

where the partial waves $\epsilon \kappa$ of the continuum electron are generated as *distorted* waves within the potential of the corresponding final ionic state. From these amplitudes $V_{i \rightarrow f, \kappa}$ of all the contributing partial waves, the AUGER program then calculates the Auger transition rate; cf. Ref. [24] for further details.

C. The MCDF method

The bound-state wave functions that are utilized for the computation of the Auger amplitudes are generated by applying the multiconfiguration Dirac–Fock (MCDF) method. Within the MCDF formalism, the atomic state function Ψ_α of an energy eigenstate α is constructed as a linear combination of so-called configuration state functions (CSFs) Φ with well-defined parity P , total angular momentum J , and projection of total angular momentum M :

$$\Psi_\alpha(PJM) = \sum_{i=1}^{n_c} c_i(\alpha) \Phi(\gamma_i PJM). \quad (7)$$

Here, n_c denotes the number of CSFs and $\{c_i(\alpha)\}$ is the representation of the atomic state within the given CSF basis. Moreover, γ_i refers to all remaining quantum numbers that are needed to uniquely specify a CSF. Usually, all n_c CSFs are constructed from a common set of orthonormal atomic orbitals, i.e., from a set with $\langle \phi_i | \phi_j \rangle = \delta_{ij}$ for each pair of orbitals.

D. Shake processes and the biorthonormal transformation

In order to model the first step of the cascade realistically, we have to consider shake processes of the initially excited np electron into shells with other principal quantum numbers n' ,

$$1s^1 2s^2 2p^6 np \rightarrow 1s^2 2s^k 2p^{6-k} n' \ell + e^-. \quad (8)$$

In a simple picture, shake processes arise from the *overlap* of the different orbitals when the initial and final states are optimized separately. In this model, a shake-up of the valence electron from 3p to 4p requires that the 3p orbital of the initial state overlaps with the 4p orbital of the final state. In zeroth approximation, the shake probability is equal to the modulus squared of this orbital overlap, while the mixing between different configurations may lead to additional contributions to the shake probabilities.

Since the initial and the final bound-state wave functions Ψ_i, Ψ_f differ in their number of electrons, the two orbital sets $\{\phi_i\}$ and $\{\phi'_i\}$ of the initial and final

states are generally *not* biorthonormal, i.e., the relation $\langle \phi_i | \phi'_j \rangle = \delta_{ij}$ does not hold. While the separately optimized single-electron orbitals are utilized within the AUGER program, this component of the RATIP package still assumes a common orthonormal set of orbitals for both the initial and the final states in the evaluation of the (angular part of the) many-electron Auger amplitudes. Therefore, in order to treat shake processes within the RATIP code, one has to account for the overlap of the initial- and final-state orbitals in a different way, for instance, by employing the biorthonormal transformation as described in Ref. [25] and implemented in the (more recent) GRASP [26] package.

In a *biorthonormal transformation*, the two sets of orbital functions are modified, $\{\phi_i\}, \{\phi'_i\} \mapsto \{\tilde{\phi}_i\}, \{\tilde{\phi}'_i\}$, such that the obtained orbitals finally fulfill the standard relation $\langle \tilde{\phi}_i | \tilde{\phi}'_j \rangle = \delta_{ij}$. Of course, any change of the orbitals also modifies the CSFs, $\Phi(\gamma_i P J M) \mapsto \tilde{\Phi}(\gamma_i P J M)$, and, hence, the representation of the atomic states in the given basis. Therefore, in order to leave the atomic state functions invariant, the coefficients $c_i \mapsto \tilde{c}_i$ need to be transformed as well to fulfill the equivalence

$$\sum_{i=1}^{n_c} c_i(\alpha) \Phi(\gamma_i P J M) = \sum_{i=1}^{n_c} \tilde{c}_i(\alpha) \tilde{\Phi}(\gamma_i P J M). \quad (9)$$

By applying a biorthonormal transformation to the atomic states, the (original) orbital overlap is now accounted for by means of the mixing of different configurations and, thus, such a transformation provides a very elegant method to deal with atomic shake processes.

III. CALCULATIONS

The suite of GRASP [26] programs was employed to generate all bound-state wave functions and to perform the biorthonormal transformation of the initial and final states for each step of the cascades. For such a biorthonormal set of orbitals, the Auger decay rates are calculated with the AUGER component of the RATIP package.

To simulate the electron spectra below, the initial resonant photoexcitation as well as all subsequent Auger electron emissions are treated as independent steps of the overall autoionization process. In particular, here we *do not* account for the alignment of the atoms due to their photoexcitation since we are only interested in the (angle-integrated) electron spectra. This is in contrast to a few recent studies on the *coherence* transfer through two (or more) overlapping resonances, and how such a transfer affects the angular distribution of the second-step Auger electrons [15, 20].

In the present study, moreover, we do also not consider any *direct* multiple Auger processes which would lead to the simultaneous emission of two or more electrons. These direct processes only occur in second- or even higher-order perturbation theory and are assumed to be negligible as

long as sequential Auger cascades are energetically possible. We also neglect all radiative decay processes which are typically suppressed by several orders of magnitude.

A. Bound-state wave function generation

As mentioned before, the first step of the cascade is strongly affected by shake-up or -down processes of the initially excited np ($n = 3, 4$) electron into shells with principal quantum numbers $n' \neq n$. In our computations, we have therefore taken into account all those configurations in which the np valence electron is displaced into one of the neighboring $n'p$ orbitals. In the wave function expansions of the intermediate and final states of the cascade, we included all $2\ell^k np$ configurations with $n = 3, \dots, 7$. Further configurations with even higher principal quantum numbers of the spectator electron were found negligible in a series of test computations. In a recent experiment by Tamenori and Suzuki [8], moreover, the *conjugate* shake processes $1s^{-1}3p \rightarrow 1s^2 2s^2 2p^4 (^1D) 3d$ have also been observed. We therefore also included the 3d orbitals in our computations to account for such conjugate shake processes.

Electron correlation effects are known to play an essential role in describing (inner-shell) excited atomic states. For this reason, we have also incorporated various states that cannot be populated during the cascade process (i.e., Ne^{2+} states whose energies are higher than the highest considered Ne^+ state) into the basis, because they often mix with the energetically low-lying states and, hence, may affect the computation of the corresponding Auger rates. To model the relevant states of neutral, singly ionized, as well as doubly ionized neon, we include all CSFs of the following configurations in our computations:

- Ne (24 CSFs): $1s^1 2s^2 2p^6 nl$,
- Ne^+ (261 CSFs): $1s^2 2s^2 2p^5$, $1s^2 2s^1 2p^6$,
 $1s^2 2s^2 2p^4 nl$, $1s^2 2s^1 2p^5 nl$, $1s^2 2s^0 2p^6 nl$,
- Ne^{2+} (516 CSFs): $1s^2 2s^2 2p^4$, $1s^2 2s^1 2p^5$,
 $1s^2 2s^2 2p^3 nl$, $1s^2 2s^0 2p^6$, $1s^2 2s^1 2p^4 nl$, $1s^2 2s^0 2p^5 nl$,

where $nl \in \{3p, 3d, 4p, 5p, 6p, 7p\}$.

B. Energy levels

The second step of the cascade includes a large number of Auger transitions with quite low energies. In order to correctly reproduce these low-energy spectra, one needs to be able to distinguish between the energetically allowed and the energetically forbidden transitions. The level energies from such *ab-initio* calculations as performed here are usually not accurate enough to make this distinction explicit. Therefore, we here make use of the experimentally known level energies of neutral, singly and doubly-charged neon, as far as available, to better reproduce the Auger

energies of the emitted electrons. In some more detail, these experimental energies were obtained from different sources:

- Energies of low-lying levels of Ne^+ (where available) and Ne^{2+} as well as the ionization energies were obtained from the NIST Atomic Spectra Database [27].
- The Auger spectra from Refs. [7, 8, 16, 17, 28] were used for determining some additional Ne^+ energy levels that are not available from optical data.
- Values for the $1s^{-1}3p$ and $1s^{-1}4p$ excitation energies were taken from Ref. [21].

For other levels, unfortunately, there is no experimental data available. Nevertheless, these level energies can still be *improved* by using the known energies of neighboring levels and applying a proper interpolation scheme.

IV. RESULTS

We now present the results of our simulation of the complete two-step Auger cascades following the resonant photoexcitation of the core-excited $1s^{-1}3p$ 1P_1 and $1s^{-1}4p$ 1P_1 levels of neutral neon. We aim to accurately predict the Auger electron spectra, the shake probabilities, as well as the ion yields.

A. The first-step single ionization spectrum

The resonantly excited $1s^{-1}np$ 1P_1 levels can decay to any of the 261 levels of Ne^+ which we consider above in Eq. (1). Here, we shall restrict our discussion to the dominant *peaks* of the calculated spectra, which may consist of one or several Auger transitions between (nearly-degenerate) fine structure levels. Fig. 2 shows the calculated Auger electron spectra for the first step of the cascade. For the sake of simplicity, we plot every electron line as a Gaussian with a constant full width at half maximum (FWHM) of 100 meV. Only peaks with a relative intensity > 0.01 (with regard to the largest peak in each spectrum) are numbered in the figure and listed in Table I.

The peaks in the spectra of Fig. 2 form several well-separated groups which are associated with different configurations of the Ne^+ ions as listed in Eq. (1). Going from low to high electron energies, we can distinguish the levels of the following final-state configurations for this first step of the cascade: Transitions to levels of the $2s^0 2p^6 nl$ configurations at 746–756 eV, $2s^1 2p^5 nl$ at 770–790 eV, $2s^2 2p^4 nl$ at 799–816 eV, $2s^1 2p^6$ at 818.7 eV, as well as to $2s^2 2p^5$ at 845.5–845.6 eV, respectively. All these electron energies refer to the decay of the $1s^{-1}3p$ resonance and are released in step (1) of the cascade. For the decay of the $1s^{-1}4p$ 1P_1 level, the Auger transitions to the same final levels of Ne^+ yield electron energies that

are about 1.6 eV higher owing to the energy difference between the $1s^{-1}3p$ and $1s^{-1}4p$ levels.

The autoionization of the $1s^{-1}3p$ 1P_1 and $1s^{-1}4p$ 1P_1 core-excited levels to the $2s^1 2p^6$ $^2S_{1/2}$ level of singly charged neon ions occurs particularly weak in our computations. For these two Auger lines, the calculated relative intensities are only about 4.7×10^{-6} and 1.2×10^{-6} compared to the largest peaks in the respective spectra. This differs from experimental findings where the transitions to the $2s^1 2p^6$ $^2S_{1/2}$ level can be clearly seen in the recorded spectra for both excitations, cf. Ref. [6]. A possible reason for this might be an inadequate expansion of the wave function for this particular level. From an analysis of the calculated energies, the $2s^1 2p^6$ $^2S_{1/2}$ level energy is indeed found about 5 eV too high with respect to the neighboring $2s^2 2p^4 3p$ levels (as obtained from optical data). This rather large deviation indicates that this $^2S_{1/2}$ level is represented rather poorly within the given basis.

The Auger transitions to various levels of the $2s^2 2p^4 nl$ configurations of Ne^+ clearly dominate the electron spectra of the first step (1). Altogether, these Auger lines make up about 75% of the total intensity for the decay of the $1s^{-1}3p$ 1P_1 and $1s^{-1}4p$ 1P_1 core-excited levels. Therefore, these groups of transitions have been explored extensively in the literature [3, 5, 6, 8] and, hence, are well suited for a comparison of our computations with experiment. In Table I, for example, we list the measured intensities by Kivimäki *et al.* [6] for the transitions to the $2s^2 2p^4 3p$ states. Since the values in Ref. [6] are normalized such that they add up to 100, we scale them appropriately. Our values compare reasonably well to the experimental intensities. Especially the intensity ratios of the dominant transitions to the $2s^2 2p^4(^1D)3p$ multiplets show very good agreement.

Fig. 3 shows the Auger electron spectra of the transitions to the $2s^2 2p^4 nl$ states of Ne^+ in greater detail. We here include recent experimental data from Ref. [8] along with our calculated spectra in order to compare the relative intensities of the recorded electron lines. (Note that, since we employ experimental energies in our computations, the transition energies naturally match the experimental values.) In the experiment [8], the Auger electron spectra were observed for both parallel and perpendicular polarization of the incident photon beam with respect to the detector axis to obtain angle-resolved spectra. Since we limit ourselves to a simulation of the (angle-integrated) intensities of the transitions with no account of the angular distribution, we determine the angle-independent intensities from the experimental data. Our calculated intensities agree well with the experimental spectra. Especially, we can predict quite accurately to which extent shake processes take place and affect the observed spectra.

Table II lists the predicted shake-up and shake-down probabilities for the initially excited 3p and 4p electrons into neighboring nl shells during the first step of the cascade. For an initial $1s^{-1}3p$ excitation, the spectator process that leaves the 3p electron in its valence shell clearly dominates with a probability of 72%. For this

TABLE I. Energies and intensities of all major electron lines in the first-step Auger electron spectra of $1s^{-1}np\ ^1P_1$ ($n = 3, 4$) excited neon. The (relative) intensities of these peaks are denoted by I_Σ and refer for each initial $1s^{-1}np\ ^1P_1$ level to the most intense peak, i.e., to peak 22 for the initial $1s^{-1}3p$ excitation and to peak 15 for $1s^{-1}4p$, respectively. For the decay of the core-excited $1s^{-1}3p\ ^1P_1$ level, the calculated intensities are compared, whenever possible, with experimental data by Kivimäki *et al.* [6]. Columns 4 and 7, moreover, display the relative intensities within each single peak, denoted by I , i.e., the fractions of a particular fine-structure line with regard to the intensity of that peak.

No.	Final level(s)	$1s^{-1}3p$ excitation				$1s^{-1}4p$ excitation		
		E_k (eV)	I	I_Σ		E_k (eV)	I	I_Σ
				This work	Expt. [6]			
1	$2s^0 2p^6 5p\ ^2P$					749.72–749.73	1.0	0.043
2	$2s^0 2p^6 4p\ ^2P$	750.06	1.0	0.032		751.69	1.0	0.016
3	$2s^0 2p^6 3p\ ^2P$	755.18	1.0	0.075				
4	$2s^1 2p^5\ (^1P)\ 5p\ ^2S_{1/2}$					773.15 ^a	0.10	0.320
	$2s^1 2p^5\ (^1P)\ 5p\ ^2P$					773.19	0.33	
	$2s^1 2p^5\ (^1P)\ 5p\ ^2D$					773.23	0.56	
5	$2s^1 2p^5\ (^1P)\ 4p\ ^2S_{1/2}$	773.40 ^a	0.10	0.233		775.03 ^a	0.13	0.121
	$2s^1 2p^5\ (^1P)\ 4p\ ^2P$	773.50	0.32			775.13	0.35	
	$2s^1 2p^5\ (^1P)\ 4p\ ^2D$	773.58–773.59	0.58			775.21–775.22	0.52	
6	$2s^1 2p^5\ (^1P)\ 3p\ ^2P$	778.56	1.0	0.191		780.19	1.0	0.013
7	$2s^1 2p^5\ (^1P)\ 3p\ ^2D$	778.82–778.83	0.83	0.369		780.45–780.46	0.87	0.026
	$2s^1 2p^5\ (^1P)\ 3p\ ^2S_{1/2}$	778.84	0.17			780.47	0.13	
8	$2s^1 2p^5\ (^3P)\ 5p\ ^2P$					783.61–783.65	0.27	0.020
	$2s^1 2p^5\ (^3P)\ 5p\ ^2D$					783.68–783.79	0.41	
	$2s^1 2p^5\ (^3P)\ 5p\ ^4P$					783.73–783.74	0.19	
	$2s^1 2p^5\ (^3P)\ 5p\ ^4D$					783.74–783.81 ^a	0.12	
9	$2s^1 2p^5\ (^3P)\ 4p\ ^2S_{1/2}$	783.70	—	0.027		785.33	0.24	0.019
	$2s^1 2p^5\ (^3P)\ 4p\ ^2P$	783.92–783.97	0.35			785.55–785.60	0.27	
	$2s^1 2p^5\ (^3P)\ 4p\ ^2D$	783.97–784.03	0.44			785.60–785.66	0.34	
	$2s^1 2p^5\ (^3P)\ 4p\ ^4P$	783.99–784.05	0.17			785.62–785.68	0.13	
	$2s^1 2p^5\ (^3P)\ 4p\ ^4D$	784.06–784.14 ^a	0.03			785.69–785.77 ^a	0.02	
10	$2s^1 2p^5\ (^3P)\ 3p\ ^2S_{1/2}$	788.19	1.0	0.016				
11	$2s^1 2p^5\ (^3P)\ 3p\ ^2P$	788.89–788.92	0.37	0.081				
	$2s^1 2p^5\ (^3P)\ 3p\ ^2D$	789.01–789.06	0.58					
	$2s^1 2p^5\ (^3P)\ 3p\ ^4P$	789.07–789.10 ^b	0.05					
12	$2s^2 2p^4\ (^1S)\ 5p\ ^2P$					802.18	1.0	0.088
13	$2s^2 2p^4\ (^1S)\ 4p\ ^2P$	802.52	1.0	0.053		804.15	1.0	0.029
14	$2s^2 2p^4\ (^1D)\ 6p\ ^2P$					804.84 ^a	0.09	0.019
	$2s^2 2p^4\ (^1D)\ 6p\ ^2D$					804.90	0.32	
	$2s^2 2p^4\ (^1D)\ 6p\ ^2F$					804.93	0.59	
15	$2s^2 2p^4\ (^1D)\ 5p\ ^2P$					805.71–805.72 ^a	0.16	1.0
	$2s^2 2p^4\ (^1D)\ 5p\ ^2D$					805.86	0.34	
	$2s^2 2p^4\ (^1D)\ 5p\ ^2F$					805.91	0.50	
16	$2s^2 2p^4\ (^3P)\ 7p$	805.85–805.99 ^a	0.02	0.721		807.48–807.62 ^a	0.02	0.381
	$2s^2 2p^4\ (^1D)\ 4p\ ^2D$	806.17	0.30			807.80	0.32	
	$2s^2 2p^4\ (^1D)\ 4p\ ^2P$	806.16–806.18	0.03			807.79–807.81	0.15	
	$2s^2 2p^4\ (^1D)\ 4p\ ^2F$	806.28	0.60			807.91	0.50	
	$2s^2 2p^4\ (^3P)\ 6p$	806.38–806.50 ^b	0.05			808.01–808.13 ^b	0.02	
17	$2s^2 2p^4\ (^3P)\ 5p\ ^2P$	807.26–807.29	0.96	0.038				
	$2s^2 2p^4\ (^3P)\ 5p\ ^2D$	807.36–807.45	0.01					
	$2s^2 2p^4\ (^3P)\ 5p\ ^4D$	807.38–807.47	0.02					
18	$2s^2 2p^4\ (^1S)\ 3p\ ^2P$	807.70	1.0	0.192	0.321	809.33	1.0	0.014
19	$2s^2 2p^4\ (^3P)\ 4p\ ^2P$	809.07–809.10	1.0	0.075				
20	$2s^2 2p^4\ (^1D)\ 3p\ ^2D$	811.18	1.0	0.744	0.725	812.81	1.0	0.052
21	$2s^2 2p^4\ (^1D)\ 3p\ ^2P$	811.28–811.31	1.0	0.333	0.373	812.91–812.94	1.0	0.021
22	$2s^2 2p^4\ (^1D)\ 3p\ ^2F$	811.54–811.55	1.0	1.0	1.0	813.17–813.18	1.0	0.076
23	$2s^2 2p^4\ (^3P)\ 3p\ ^2P$	814.04–814.05	1.0	0.043	0.027			
24	$2s^2 2p^5\ ^2P$	845.47–845.57	1.0	0.017				

^a The energies of these transitions are not known from experimental data.

^b The energies of some of these transitions are not known from experimental data.

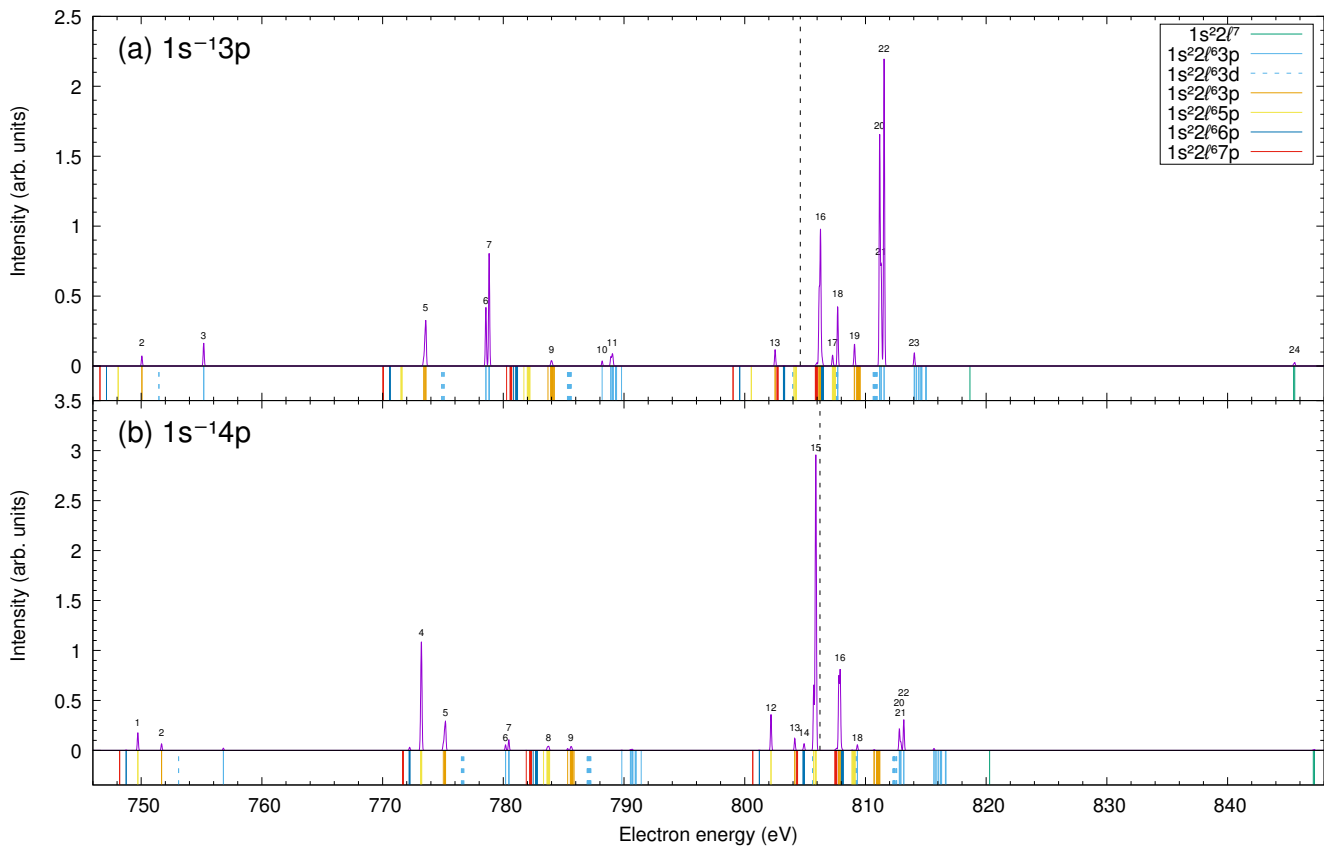


FIG. 2. Simulated Auger electron spectra for the first step (1) of the cascade due to the decay of the core-excited (a) $1s^{-1}3p \ ^1P_1$ and (b) $1s^{-1}4p \ ^1P_1$ levels. Every electron line is plotted as a Gaussian with a constant 100 meV FWHM. Peaks with a sufficiently large intensity are labeled with the same numbers as used for indexing in the first column of Table I. The vertical lines below the plots indicate all possible electron transitions in this cascade, where the colors correspond to different final-state configurations, cf. the legend. The two vertical lines at (a) 804.6 eV and (b) 806.2 eV represent the double ionization threshold: the spectral lines to the left of these dashed lines represent transitions to singly-ionized levels with energies above the Ne^{2+} ground state that typically take part in the second step of the cascade.

TABLE II. Calculated shake probabilities for the first step of the cascade. Recent experimental values obtained by Tamenori and Suzuki [8] are given for comparison.

Final orbital	$1s^{-1}3p$ excitation		$1s^{-1}4p$ excitation	
	This work	Expt. [8]	This work	Expt. [8]
3p	0.72	} 0.69	0.096	} 0.08
3d	2.9×10^{-4}		5.6×10^{-5}	
4p	0.26	0.31	0.24	0.26
5p	0.0099	< 0.01	0.64	0.64
6p	0.0085	< 0.01	0.015	0.02
7p	0.0036	< 0.01	0.0033	< 0.01

initial resonance, the shake-up to the 4p orbital has a probability of 26%, while the shake-ups into even higher shells are rather weak with respective probabilities < 1%. For an initial $1s^{-1}4p$ excitation, in contrast, the shake-up to 5p dominates with a probability of 64% over the

spectator process (24%). Other notable shake processes are the shake-down to 3p (9.6%) and the shake-up to 6p (1.5%). Our calculated shake probabilities agree very well with the experimental findings from Ref. [8].

To predict these shake probabilities, we use the calculated intensities from above and sum over all those intensities that belong to a particular spectator orbital. When we just consider the overall shake probabilities, quite good results (cf. e.g. the calculated values in Ref. [3]) are also obtained by just taking the modulus squared of the orbital overlaps. However, if we need to determine the shake probabilities for some specific transition, this approach is no longer appropriate as one observes significant differences for final levels (terms) that are coupled differently. For example, significant deviations occur for the transitions from the initial $1s^{-1}3p \ ^1P_1$ level to the $2s^2 2p^4(^3P)3p \ ^2P$ and $2s^2 2p^4(^1S)3p \ ^2P$ doublets (peaks 23 and 18) when compared to the corresponding shake-up transitions to the $2s^2 2p^4(^3P)4p \ ^2P$ and $2s^2 2p^4(^1S)4p \ ^2P$ doublets (peaks 19 and 13), respectively. While a shake-up to the $2s^2 2p^4(^3P)4p \ ^2P$ doublet is almost twice as

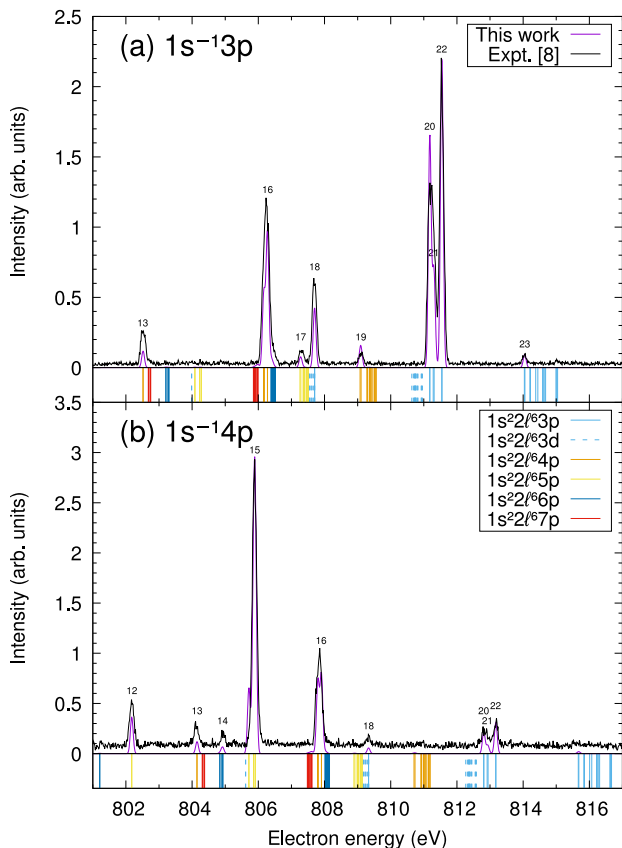


FIG. 3. Comparison of the theoretical and experimental electron spectra. Results from the experiment by Tamenori and Suzuki [8] are shown together with an enlarged part of the simulated spectra from Fig. 2 for (a) the $1s^{-1}3p$ 1P_1 and (b) the $1s^{-1}4p$ 1P_1 levels.

likely as the spectator decay to the $2s^22p^4(^3P)3p$ 2P doublet (0.075 : 0.043, cf. Table I), a shake-up to the $2s^22p^4(^1S)4p$ 2P doublet is 4 times *less* likely compared to the transitions to the corresponding $2s^22p^4(^1S)3p$ 2P doublet (0.053 : 0.192).

According to our calculations, the population of the 3d subshell via a conjugate shake process is strongly suppressed and almost negligible. In Ref. [8], however, the small peak at 807.3 eV in the $1s^{-1}3p$ spectrum (peak 17 in Fig. 3) has been assigned to the $1s^{-1}3p \rightarrow 2s^22p^4(^1D)3d$ transitions. Based on our computations, we instead propose that the observed peak belongs to the $1s^{-1}3p \rightarrow 2s^22p^4(^3P)5p$ (normal) shake transitions. The calculated intensity of the $(^3P)5p$ transitions exceeds that of the $(^1D)3d$ transitions by about two orders of magnitude, and also the well-known energies of the $2s^22p^4(^1D)3d$ and $(^3P)5p$ levels (as obtained from optical data [27]) suggest that the observed electron lines correspond to the $2s^22p^4(^3P)5p$ levels of the Ne^+ ions.

In Fig. 2, the dashed vertical lines represent the double ionization threshold. All Auger transitions with an electron energy higher than this threshold populate Ne^+ levels that lie energetically below the Ne^{2+} ground level and,

TABLE III. Calculated ion yields for the decay of the resonantly excited Ne $1s^{-1}np$ 1P_1 levels ($n = 3, 4$) and comparison with experimental values obtained by Morgan *et al.* [29].

Charge	$1s^{-1}3p$ excitation		$1s^{-1}4p$ excitation	
	This work	Expt. [29]	This work	Expt. [29]
Ne^+	0.74	0.65(02)	0.24	0.24(03)
Ne^{2+}	0.26	0.31(02)	0.76	0.71(04)
Ne^{3+}	—	0.03(01)	—	0.04(01)
Ne^{4+}	—	0.002	—	0.002

hence, cannot autoionize further. On the other hand, all electron lines below this threshold correspond to autoionizing Ne^+ levels which may decay to Ne^{2+} via one of the second-step transitions listed in Eq. (2). The relative ion yields for Ne^+ and Ne^{2+} are therefore given (in very good approximation) by the intensity ratio of all peaks above and below the threshold. Table III displays the calculated ion yields. The large difference between the ion yields for the $1s^{-1}3p$ and $1s^{-1}4p$ excitations arises mainly from the different population of the $2s^22p^4(^1D)5p$ levels in the first step of the cascade. These levels lie 0.3–0.5 eV above the double ionization threshold and are dominantly populated in the first-step Auger decay following the $1s^{-1}4p$ excitation, while their population is negligible for an initial $1s^{-1}3p$ excitation. Our results for the ion yields agree quite satisfyingly with the experimental data by Morgan *et al.* [29] which is shown for comparison in Table III. While triply and even quadruply charged neon ions have been observed in the experiment [29], they require higher-order processes, such as direct double and triple Auger electron emissions or shake-up processes of two or more electrons, and are thus not included in the present study.

B. The second-step double ionization spectrum

The second-step Auger electron spectra span the energy range between 0 and 59 eV and comprise a total of 1512 transitions between fine-structure levels of Ne^+ and Ne^{2+} . About 800 of these lines have low electron energies (< 10 eV). Fig. 4 displays the calculated Auger electron spectra for step (2) of the cascade. Large parts of these spectra have been explored before with emphasis on different aspects [8, 16, 17]. While the dominant peaks are all situated below 35 eV, some additional peaks occur in the range between 42 and 59 eV. In the following, we shall therefore separately discuss three parts of the spectrum with energies 0–8 eV, 8–35 eV, and 42–59 eV, respectively.

Table IV lists all the significant peaks with energies below 8 eV together with their relative intensities. This part of the spectra is dominated by so-called *multiplet-changing Auger transitions* [30] in which the energy required for the release of the Auger electron does not arise from a change in the shell occupation (electron configuration)

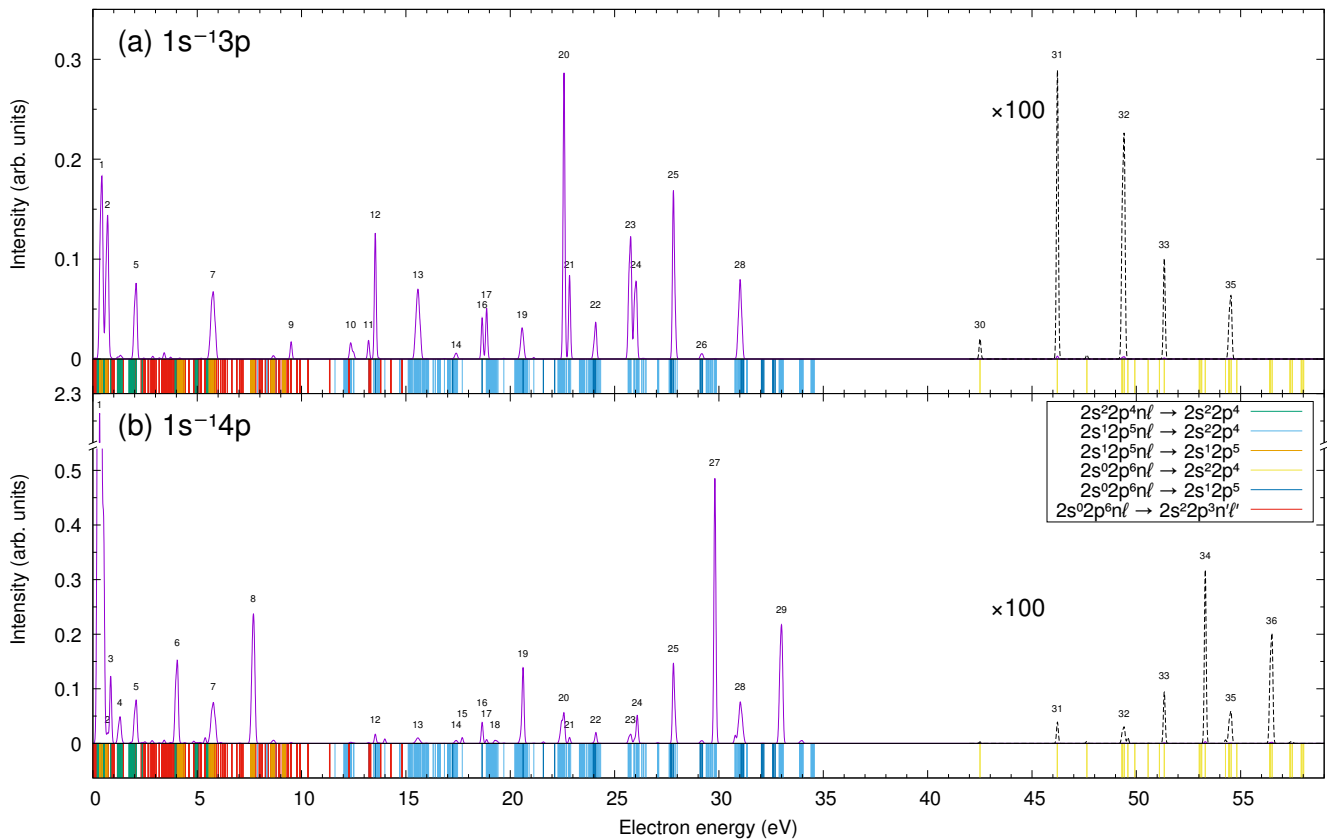


FIG. 4. The same as Fig. 2 but for the second step (2) of the Auger cascade. Peaks with a sufficiently large intensity are labeled again with numbers that refer to the numbers in the first columns of Tables IV, V, and VI. The colors of the vertical lines below the plots correspond to different initial and final configurations as shown in the legend. For electron energies higher than 42 eV, the peaks are enhanced by a factor of 100 to make the $2s^02p^6nl \rightarrow 2s^22p^4$ transitions visible.

but from the coupling of different terms of the remaining ion, i.e., a change of the multiplet coupling of the underlying parent state. For this reason, the Auger electrons in these transitions are typically emitted with very low energy. In the second step (2) of the neon cascade, the following multiplet-changing transitions are energetically allowed: The $2s^22p^4(^1D)5p$, $(^1D)6p$, $(^1D)7p$, $(^1S)3d$, and $(^1S)4p$ states of Ne^+ can decay to the $2s^22p^4\ ^3P$ states of Ne^{2+} , while the $2s^22p^4(^1S)5p$, $(^1S)6p$, and $(^1S)7p$ states can decay to the $2s^22p^4\ ^3P$ and 1D_2 states. Furthermore, all of the considered $2s^12p^5(^1P)nl$ states can decay to the $2s^12p^5\ ^3P$ states.

In addition to the multiplet-changing transitions, many of the $2s^02p^6nl \rightarrow 2s^22p^3n'l'$ shake transitions also lie in this energy range. In further detail, the energetically allowed final states here include all of the $2s^22p^33p$ and $2s^22p^33d$ states as well as the $2s^22p^3(^4S)4p$ and $2s^22p^3(^4S)5p$ states, cf. Fig. 1 above. As expected, these transitions are generally very weak, since, in addition to the low population of the $2s^02p^6nl$ levels, these second-step transitions require a conjugate shake-down $2p \rightarrow 2s$ and are, hence, strongly suppressed compared to the normal Auger transitions to the $2s^12p^5$ levels. These transitions are therefore hard to detect as they occupy just the

same energy region as the comparatively strong multiplet-changing transitions. Until now, these shake-down transitions have not been observed experimentally. Nevertheless, some of the peaks in Table IV show some minor contributions from these lines.

The intensities I_Σ of the peaks listed in Table IV are given relative to the total intensity of the two peaks 20 and 21 for the $1s^{-1}3p$ excitation and relative to peak 27 for the $1s^{-1}4p$ excitation. We have chosen this normalization for the $1s^{-1}3p$ peaks because we wish to compare the intensities for the 8–35 eV energy range with experimental values which are normalized the same way. In order to be still able to compare the intensities of peaks from different energy ranges, we shall use these peaks above for normalizing the whole second-step spectra. Although, for the initial $1s^{-1}4p$ excitation, peak 1 of the second-step spectrum is apparently the largest, we here choose peak 27 as reference because the spectrum with electron energies > 5 eV has been explored earlier in great detail (e.g., Ref. [17]), in contrast to the very-low-energy part. Peak 27 is taken as reference since it is the largest in this range of kinetic energies above 5 eV.

Unfortunately, it is difficult to assess the accuracy of the calculated intensities for these low-energy transitions.

TABLE IV. The same as in Table I but for the second-step Auger electron lines with energies between 0–8 eV. Here, the relative intensities I_{Σ} refer to peaks 20+21 for the $1s^{-1}3p$ excitation and to peak 27 for $1s^{-1}4p$, cf. Table V.

No.	Initial level(s)	Final level(s)	E_k (eV)	$1s^{-1}3p$		$1s^{-1}4p$	
				I	I_{Σ}	I	I_{Σ}
1	$2s^2 2p^4 (^1D) 5p ^2F$	$2s^2 2p^4 ^3P$	0.21–0.33	—	0.793	0.50	7.901
	$2s^2 2p^4 (^1D) 5p ^2D$	$2s^2 2p^4 ^3P$	0.26–0.37	0.01	—	0.34	—
	$2s^1 2p^5 (^1P) 3p ^2S_{1/2}$	$2s^1 2p^5 ^3P$	0.32–0.43	0.46	—	—	—
	$2s^1 2p^5 (^1P) 3p ^2D$	$2s^1 2p^5 ^3P$	0.34–0.45	0.51	—	0.01	—
	$2s^2 2p^4 (^1D) 5p ^2P$	$2s^2 2p^4 ^3P$	0.40–0.52 ^c	0.01	—	0.16	—
2	$2s^0 2p^6 6p ^2P$	$2s^2 2p^3 (^2P) 3d ^3P$	0.64–0.66	—	0.568	0.01	0.053
	$2s^1 2p^5 (^1P) 3p ^2P$	$2s^1 2p^5 ^3P$	0.60–0.72	1.0	—	0.99	—
3	$2s^2 2p^4 (^1S) 5p ^2P$	$2s^2 2p^4 ^1D_2$	0.85	—	—	0.99	0.235
	$2s^0 2p^6 4p ^2P$	$2s^2 2p^3 (^2P) 3p ^1S_0$	0.86	—	—	0.01	—
4	$2s^2 2p^4 (^1D) 6p ^2F$	$2s^2 2p^4 ^3P$	1.19–1.31	—	—	0.58	0.146
	$2s^2 2p^4 (^1D) 6p ^2D$	$2s^2 2p^4 ^3P$	1.22–1.33	—	—	0.32	—
	$2s^2 2p^4 (^1D) 6p ^2P$	$2s^2 2p^4 ^3P$	1.28–1.40 ^c	—	—	0.09	—
5	$2s^2 2p^4 (^1S) 6p ^2P$	$2s^2 2p^4 ^1D_2$	1.82	—	0.318	0.01	0.236
	$2s^0 2p^6 5p ^2P$	$2s^2 2p^3 (^2D) 3d ^1F_3$	1.84	—	—	0.01	—
	$2s^2 2p^4 (^1S) 4p ^2P$	$2s^2 2p^4 ^3P$	1.97–2.09	1.0	—	0.96	—
	$2s^0 2p^6 5p ^2P$	$2s^2 2p^3 (^2D) 3d ^1P_1$	2.07	—	—	0.02	—
6	$2s^2 2p^4 (^1S) 5p ^2P$	$2s^2 2p^4 ^3P$	3.94–4.06	—	—	1.0	0.458
7	$2s^1 2p^5 (^1P) 4p ^2D$	$2s^1 2p^5 ^3P$	5.58–5.69	0.23	0.408	0.18	0.320
	$2s^0 2p^6 5p ^2P$	$2s^2 2p^3 (^2P) 3p ^3S_1$	5.69	—	—	0.02	—
	$2s^1 2p^5 (^1P) 4p ^2P$	$2s^1 2p^5 ^3P$	5.66–5.77	0.44	—	0.41	—
	$2s^1 2p^5 (^1P) 4p ^2S_{1/2}$	$2s^1 2p^5 ^3P$	5.76–5.87 ^c	0.32	—	0.39	—
8	$2s^1 2p^5 (^1P) 5p ^2D$	$2s^1 2p^5 ^3P$	7.56–7.67	—	—	0.21	0.744
	$2s^1 2p^5 (^1P) 5p ^2P$	$2s^1 2p^5 ^3P$	7.60–7.72	—	—	0.44	—
	$2s^1 2p^5 (^1P) 5p ^2S_{1/2}$	$2s^1 2p^5 ^3P$	7.64–7.76 ^c	—	—	0.35	—

^c The energies of these Auger lines are not known from experimental data.

Previous experimental studies have investigated this low-energy part, e.g., Refs. [8, 17]. While these experimental findings agree very well with our computations for the identification of the dominant peaks in the spectra (apart from peak 2, cf. below), no quantitative analysis has been performed so far for the intensity ratios between these peaks.

In Ref. [8], the lines with energies of 0.60–0.72 eV in the second-step spectra (peak 2 in our spectra) have been attributed to the $2s^2 2p^4 (^1S) 3d \rightarrow 2s^2 2p^4 ^3P$ transitions. Since the $2s^2 2p^4 (^1S) 3d$ levels are populated only marginally during the first step, these transitions are very weak in our simulated spectra. Based on the analysis of both steps of the cascade, we propose that the observed peaks likely belong to the $2s^1 2p^5 (^1P) 3p \rightarrow 2s^1 2p^5 ^3P$ transitions instead, since the computed intensity of these transitions exceeds that of the $2s^2 2p^4 (^1S) 3d \rightarrow 2s^2 2p^4 ^3P$ transitions by five orders of magnitude. Energies for the $2s^1 2p^5 (^1P) 3p$ levels are not known from optical data but can be derived from the data in Ref. [28] under the assumption that the assignments in this reference (which were obtained by comparing the measured branching ratios and anisotropy parameters with MCDF calculations) are correct. Using these values for the $2s^1 2p^5 (^1P) 3p$ en-

ergies, one obtains Auger electron energies between 0.32 and 0.72 eV for the $2s^1 2p^5 (^1P) 3p \rightarrow 2s^1 2p^5 ^3P$ transitions, which fits well to the experimentally observed peaks.

In the higher-energy part of the second-step spectra, the $2s^1 2p^5 nl \rightarrow 2s^2 2p^4$ and $2s^0 2p^6 nl \rightarrow 2s^1 2p^5$ Auger transitions dominate in the range from 8 to 35 eV. At energies below 15 eV, also some of the $2s^1 2p^5 (^1P) nl \rightarrow 2s^1 2p^5 ^3P$ and $2s^0 2p^6 nl \rightarrow 2s^2 2p^3 n'l'$ transitions occur, but with rather small contributions. For this part of the spectra, the energies and relative intensities are listed in Table V and compared with the experiment from Ref. [16] for the initial $1s^{-1}3p$ excitation. Good quantitative agreement is found between experiment and simulations for all dominant transitions in the $1s^{-1}3p$ spectrum. In Ref. [16], however, the peaks 11+12, 14+15, 16+17, 20+21, and 23+24 were grouped together and, hence, we here provide the combined intensities of these peaks in Table V. For some of the *weak* peaks, the simulated and experimental intensities deviate up to a factor 5, especially for the peaks 10, 14+15, and 26. For the $1s^{-1}4p$ excitation, we find good qualitative agreement with the recorded spectrum from Ref. [17].

Table V also compares the intensity ratios I of the individual Auger lines with experimental data whenever

TABLE V. The same as in Table IV but for the second-step Auger electron lines with energies between 8–35 eV. For the $1s^{-1}3p$ excitation, the relative intensities measured by Yoshida *et al.* [16] are shown for comparison.

No.	Initial level(s)	Final level(s)	E_k (eV)	$1s^{-1}3p$				$1s^{-1}4p$	
				This work		Expt. [16]		I	I_Σ
				I	I_Σ	I	I_Σ		
9	$2s^1 2p^5 ({}^3P) 3p {}^2S_{1/2}$	$2s^2 2p^4 {}^1S_0$	9.50	1.0	0.046	—	—	—	—
10	$2s^1 2p^5 ({}^3P) 3p {}^4P$	$2s^2 2p^4 {}^1D_2$	12.30–12.32 ^e	0.03	0.072	0.02(02)	0.22(02)	—	—
	$2s^1 2p^5 ({}^3P) 3p {}^2D$	$2s^2 2p^4 {}^1D_2$	12.34–12.39	0.72	—	0.49	—	—	—
	$2s^1 2p^5 ({}^3P) 3p {}^2P$	$2s^2 2p^4 {}^1D_2$	12.48–12.51	0.25	—	0.39(13)	—	—	—
11+12	$2s^1 2p^5 ({}^3P) 3p {}^2S_{1/2}$	$2s^2 2p^4 {}^1D_2$	13.21	0.13	0.395	0.16(01)	0.58(04)	0.07	0.038
	$2s^0 2p^6 3p {}^2P$	$2s^1 2p^5 {}^1P_1$	13.53	0.86	—	0.80(04)	—	0.86	—
	$2s^1 2p^5 ({}^3P) 4p {}^4P$	$2s^2 2p^4 {}^1S_0$	13.64–13.70	—	—	n/a ^g	—	0.02	—
	$2s^1 2p^5 ({}^3P) 4p {}^2D$	$2s^2 2p^4 {}^1S_0$	13.66–13.72	0.01	—	n/a ^g	—	0.04	—
	$2s^1 2p^5 ({}^3P) 4p {}^2P$	$2s^2 2p^4 {}^1S_0$	13.72–13.77	—	—	n/a ^g	—	0.01	—
13	$2s^1 2p^5 ({}^3P) 3p {}^4P$	$2s^2 2p^4 {}^3P$	15.39–15.53 ^e	0.05	0.401	—	0.44(03)	0.05	0.040
	$2s^1 2p^5 ({}^3P) 3p {}^2D$	$2s^2 2p^4 {}^3P$	15.43–15.60	0.55	—	0.8 ^f	—	0.50	—
	$2s^1 2p^5 ({}^3P) 5p {}^4D$	$2s^2 2p^4 {}^1S_0$	15.51–15.58 ^d	—	—	—	—	0.01	—
	$2s^1 2p^5 ({}^3P) 5p {}^4P$	$2s^2 2p^4 {}^1S_0$	15.58–15.59	—	—	—	—	0.02	—
	$2s^1 2p^5 ({}^3P) 5p {}^2D$	$2s^2 2p^4 {}^1S_0$	15.53–15.64	—	—	—	—	0.06	—
	$2s^1 2p^5 ({}^3P) 3p {}^2P$	$2s^2 2p^4 {}^3P$	15.57–15.71	0.40	—	0.4 ^f	—	0.35	—
	$2s^1 2p^5 ({}^3P) 5p {}^2P$	$2s^2 2p^4 {}^1S_0$	15.67–15.71	—	—	—	—	0.01	—
	$2s^0 2p^6 3d {}^2D$	$2s^1 2p^5 {}^1P_1$	17.24	0.04	0.024	n/a ^g	0.12(01)	—	0.036
14+15	$2s^1 2p^5 ({}^3P) 4p {}^4D$	$2s^2 2p^4 {}^1D_2$	17.25–17.34 ^d	0.01	—	n/a ^g	—	—	—
	$2s^1 2p^5 ({}^3P) 4p {}^4P$	$2s^2 2p^4 {}^1D_2$	17.35–17.41	0.15	—	0.09(01)	—	0.07	—
	$2s^1 2p^5 ({}^3P) 4p {}^2D$	$2s^2 2p^4 {}^1D_2$	17.36–17.43	0.42	—	0.31(02)	—	0.21	—
	$2s^1 2p^5 ({}^3P) 7p {}^2S_{1/2}$	$2s^2 2p^4 {}^1S_0$	17.42 ^d	0.09	—	n/a ^g	—	0.01	—
	$2s^1 2p^5 ({}^3P) 4p {}^2P$	$2s^2 2p^4 {}^1D_2$	17.42–17.48	0.27	—	0.30(02)	—	0.13	—
	$2s^1 2p^5 ({}^3P) 4p {}^2S_{1/2}$	$2s^2 2p^4 {}^1D_2$	17.70	0.01	—	0.08(01)	—	0.57	—
	$2s^0 2p^6 4p {}^2P$	$2s^0 2p^5 {}^1P_1$	18.65	0.45	0.248	0.98(05)	0.23(02)	0.85	0.087
	$2s^1 2p^5 ({}^1P) 3p {}^2S_{1/2}$	$2s^2 2p^4 {}^1S_0$	18.85	0.01	—	n/a ^g	—	—	—
18	$2s^1 2p^5 ({}^3P) 5p {}^4D$	$2s^2 2p^4 {}^1D_2$	19.22–19.29 ^d	—	—	—	—	0.09	0.020
	$2s^1 2p^5 ({}^3P) 5p {}^4P$	$2s^2 2p^4 {}^1D_2$	19.28–19.30	—	—	—	—	0.20	—
	$2s^1 2p^5 ({}^3P) 5p {}^2D$	$2s^2 2p^4 {}^1D_2$	19.24–19.34	—	—	—	—	0.48	—
	$2s^1 2p^5 ({}^3P) 5p {}^2P$	$2s^2 2p^4 {}^1D_2$	19.38–19.41	—	—	—	—	0.23	—
19	$2s^1 2p^5 ({}^3P) 4p {}^4D$	$2s^2 2p^4 {}^3P$	20.34–20.54 ^d	0.03	0.137	—	0.22(02)	0.01	0.316
	$2s^1 2p^5 ({}^3P) 4p {}^4P$	$2s^2 2p^4 {}^3P$	20.44–20.61	0.17	—	0.1 ^f	—	0.05	—
	$2s^1 2p^5 ({}^3P) 4p {}^2D$	$2s^2 2p^4 {}^3P$	20.45–20.63	0.43	—	0.4 ^f	—	0.13	—
	$2s^1 2p^5 ({}^3P) 6p {}^2S_{1/2}$	$2s^2 2p^4 {}^1D_2$	20.55	0.01	—	—	—	—	—
	$2s^1 2p^5 ({}^3P) 4p {}^2P$	$2s^2 2p^4 {}^3P$	20.51–20.68	0.36	—	0.6 ^f	—	0.11	—
	$2s^0 2p^6 5p {}^2P$	$2s^1 2p^5 {}^1P_1$	20.62	—	—	—	—	0.69	—
20+21	$2s^1 2p^5 ({}^3P) 5p {}^4P$	$2s^2 2p^4 {}^3P$	22.37–22.50	—	1.0	—	1.0	0.11	0.226
	$2s^1 2p^5 ({}^3P) 5p {}^4D$	$2s^2 2p^4 {}^3P$	22.31–22.50 ^d	—	—	—	—	0.08	—
	$2s^1 2p^5 ({}^3P) 5p {}^2D$	$2s^2 2p^4 {}^3P$	22.33–22.55	—	—	—	—	0.23	—
	$2s^1 2p^5 ({}^3P) 5p {}^2P$	$2s^2 2p^4 {}^3P$	22.47–22.62	—	—	—	—	0.16	—
	$2s^1 2p^5 ({}^1P) 3p {}^2D$	$2s^2 2p^4 {}^1D_2$	22.57–22.58	0.77	—	0.94(05)	—	0.33	—
	$2s^1 2p^5 ({}^1P) 3p {}^2P$	$2s^2 2p^4 {}^1D_2$	22.84	0.23	—	0.06(01)	—	0.09	—
	$2s^0 2p^6 3p {}^2P$	$2s^1 2p^5 {}^3P$	23.98–24.10	0.58	0.133	1.0 ^f	0.22(02)	0.17	0.042
22	$2s^1 2p^5 ({}^1P) 4p {}^2D$	$2s^2 2p^4 {}^1S_0$	24.10–24.11	0.42	—	—	—	0.82	—
	$2s^1 2p^5 ({}^1P) 4p {}^2S_{1/2}$	$2s^2 2p^4 {}^1S_0$	24.29 ^d	—	—	—	—	0.01	—
	$2s^1 2p^5 ({}^1P) 3p {}^2D$	$2s^2 2p^4 {}^3P$	25.66–25.78	0.60	0.860	0.3 ^f	0.85(05)	0.30	0.170
23+24	$2s^1 2p^5 ({}^1P) 3p {}^2P$	$2s^2 2p^4 {}^3P$	25.93–26.05	0.40	—	0.7 ^f	—	0.19	—
	$2s^1 2p^5 ({}^1P) 5p {}^2D$	$2s^2 2p^4 {}^1S_0$	26.09	—	—	—	—	0.51	—
	$2s^1 2p^5 ({}^1P) 4p {}^2D$	$2s^2 2p^4 {}^1D_2$	27.81	0.79	0.555	0.97(05)	0.53(04)	0.76	0.353
25	$2s^1 2p^5 ({}^1P) 4p {}^2P$	$2s^2 2p^4 {}^1D_2$	27.90	0.21	—	0.03(01)	—	0.24	—
	$2s^0 2p^6 4p {}^2P$	$2s^1 2p^5 {}^3P$	29.10–29.22	1.0	0.022	0.9 ^f	0.12(01)	—	—
27	$2s^1 2p^5 ({}^1P) 5p {}^2D$	$2s^2 2p^4 {}^1D_2$	29.80	—	—	—	—	0.79	1.0
	$2s^1 2p^5 ({}^1P) 5p {}^2P$	$2s^2 2p^4 {}^1D_2$	29.84	—	—	—	—	0.21	—
28	$2s^1 2p^5 ({}^1P) 6p {}^2D$	$2s^2 2p^4 {}^1D_2$	30.77	—	0.370	—	0.36(03)	0.08	0.318
	$2s^1 2p^5 ({}^1P) 6p {}^2P$	$2s^2 2p^4 {}^1D_2$	30.81	—	—	—	—	0.02	—
	$2s^1 2p^5 ({}^1P) 4p {}^2D$	$2s^2 2p^4 {}^3P$	30.90–31.02	0.59	—	0.4 ^f	—	0.42	—
	$2s^1 2p^5 ({}^1P) 4p {}^2P$	$2s^2 2p^4 {}^3P$	30.99–31.10	0.41	—	0.6 ^f	—	0.35	—
	$2s^0 2p^6 5p {}^2P$	$2s^1 2p^5 {}^3P$	31.07–31.18	—	—	—	—	0.14	—
29	$2s^1 2p^5 ({}^1P) 5p {}^2D$	$2s^2 2p^4 {}^3P$	32.89–33.00	—	—	—	—	0.56	0.677
	$2s^1 2p^5 ({}^1P) 5p {}^2P$	$2s^2 2p^4 {}^3P$	32.93–33.04	—	—	—	—	0.44	—

^d The energies of these Auger lines are not known from experimental data.

^e The energies of some of these Auger lines are not known from experimental data.

^f These values are based on the best fit to the observed peak structure and are considered tentative [16].

^g These intensities cannot be established since the observed peaks are not assigned to a specific transition in Ref. [16].

TABLE VI. The same as in Table IV but for the second-step Auger electron lines with energies between 42–59 eV.

No.	Initial level(s)	Final level(s)	E_k (eV)	$1s^{-1}3p$		$1s^{-1}4p$	
				I	I_Σ	I	I_Σ
30	$2s^0 2p^6 3p \ ^2P$	$2s^2 2p^4 \ ^1S_0$	42.51	1.0	0.000 55		
31	$2s^0 2p^6 3p \ ^2P$	$2s^2 2p^4 \ ^1D_2$	46.21–46.22	1.0	0.007 81	1.0	0.000 74
32	$2s^0 2p^6 3p \ ^2P$	$2s^2 2p^4 \ ^3P$	49.30–49.42	1.0	0.009 73	0.81	0.001 14
	$2s^0 2p^6 5p \ ^2P$	$2s^2 2p^4 \ ^1S_0$	49.59–49.60	—		0.19	
33	$2s^0 2p^6 4p \ ^2P$	$2s^2 2p^4 \ ^1D_2$	51.34	1.0	0.002 72	1.0	0.001 79
34	$2s^0 2p^6 5p \ ^2P$	$2s^2 2p^4 \ ^1D_2$	53.30			1.0	0.006 09
35	$2s^0 2p^6 6p \ ^2P$	$2s^2 2p^4 \ ^1D_2$	54.27	—	0.002 71	0.06	0.001 91
	$2s^0 2p^6 4p \ ^2P$	$2s^2 2p^4 \ ^3P$	54.43–54.54	1.0		0.94	
36	$2s^0 2p^6 5p \ ^2P$	$2s^2 2p^4 \ ^3P$	56.39–56.51			1.0	0.006 08

possible. Although the fine structure of the 3P multiplets was resolved in the experiment [16], we here present the combined intensities of the transitions to the 3P levels in order to keep the size of Table V feasible. In practice, however, the comparison with the experimental intensities I is not always simple as no assignments were made for some of the observed peaks. We denote these cases by “n/a” in Table V. For some other peaks, moreover, the intensity ratios of the contributing transitions cannot be resolved and were just estimated by a fit. The uncertainties of these intensities are believed to be of the order of the reported values [16]. These values are quoted in Table V for the sake of completeness and are marked appropriately. While very good agreement is found especially for peaks 11+12 and 14+15, some larger deviations occur for other peaks. This applies especially to the peaks 16 and 17, which have similar intensities in our computations, while peak 16 clearly dominates experimentally.

The spectrum between 42–59 eV comprises the $2s^0 2p^6 nl \rightarrow 2s^2 2p^4$ transitions. These transitions are generally weak when compared with the decay to the $2s^1 2p^5$ levels and are two orders of magnitude less intense than the major peaks at 8–35 eV. This behavior is expected since these transitions include a conjugate shake-down $2p \rightarrow 2s$, similar to the $2s^0 2p^6 nl \rightarrow 2s^2 2p^3 nl$ transitions. They have not yet been observed experimentally. In order to make them visible in our simulated spectrum in Fig. 4, they are enlarged by a factor of 100. The transitions that make up the labeled peaks are listed in Table VI.

From the analysis of the electron spectra, we can also derive the population of final states of each step of the cascade. For the first step, the relative population of final Ne^+ levels can be directly obtained from the (computed) Auger rates since the initial $1s^{-1}np \ ^1P_1$ level is the same for all transitions.

For the second step of the cascade, in contrast, the rather large number of *initial* states then leads to a final-state distribution that is less obvious. Fig. 5 shows the relative population of the energy levels of Ne^{2+} after the second step of the cascade. Moreover, Table VII lists the

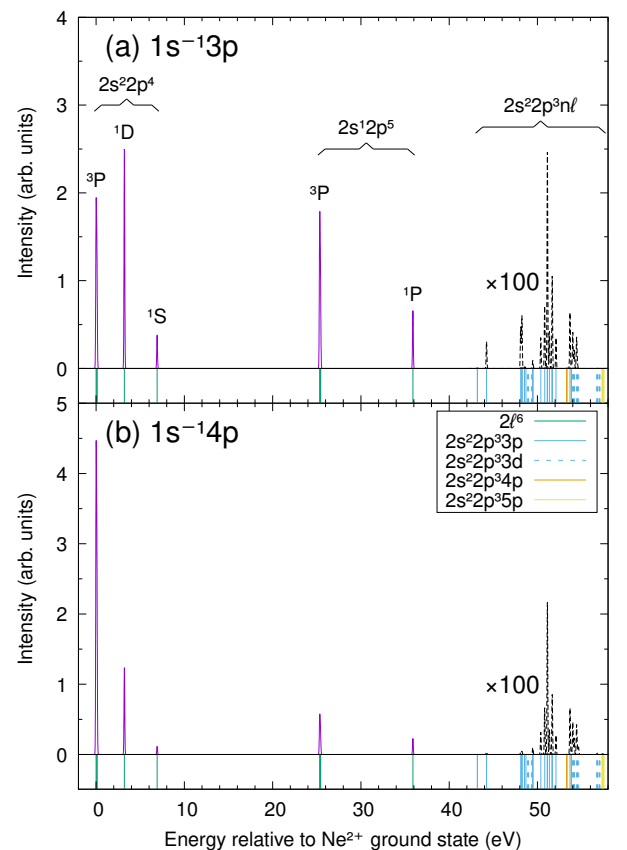


FIG. 5. Simulated population of the Ne^{2+} energy levels for the (a) $1s^{-1}3p \ ^1P_1$ and (b) $1s^{-1}4p \ ^1P_1$ excitations. The part of the spectra that belong to the $2s^2 2p^3 nl$ levels is enhanced by a factor of 100 in order to make the population of these levels visible.

relative population per fine-structure multiplet for the $2s^2 2p^4$ and $2s^1 2p^5$ levels, and just per configuration for the (less populated) $2s^2 2p^3 nl$ levels. Experimentally, such a final state distribution is obtained quite easily if all the emitted electrons are recorded in coincidence, like in a

TABLE VII. Relative population of the final Ne^{2+} energy levels after the second step (2) of the cascade. The energies are given relative to the $\text{Ne}^{2+} 2s^2 2p^4 \ ^3P_2$ ground level.

Level(s)	Energy (eV)	Relative population	
		$1s^{-1}3p$	$1s^{-1}4p$
$2s^2 2p^4 \ ^3P$	0.00–0.11	0.33	0.73
$2s^2 2p^4 \ ^1D_2$	3.20	0.27	0.13
$2s^2 2p^4 \ ^1S_0$	6.91	0.040	0.012
$2s^1 2p^5 \ ^3P$	25.33–25.44	0.29	0.093
$2s^1 2p^5 \ ^1P_1$	35.89	0.070	0.024
$2s^2 2p^3 3p$	43.20–53.69	0.0080	0.0059
$2s^2 2p^3 3d$	48.93–57.40	0.0011	0.0014
$2s^2 2p^3(^4S)4p$	53.32–53.85	4.1×10^{-5}	3.0×10^{-5}
$2s^2 2p^3(^4S)5p$	57.34–57.51	5.0×10^{-9}	5.5×10^{-8}

magnetic bottle, cf. e.g. Ref. [18] for a recent study of triple ionization of atomic cadmium.

The second step (2) of the cascades leads with a probability of $> 99\%$ to one of the levels of the $2s^2 2p^4$ or $2s^1 2p^5$ configuration. Since the higher-lying $2s^2 2p^3 n\ell$ levels can only be populated via the rare $2s^0 2p^6 n\ell \rightarrow 2s^2 2p^3 n'\ell'$ transitions, their population remains almost negligible. Out of these $2p^2 2p^3 n\ell$ levels, several $3p$ and $3d$ levels are predominantly populated, while the population of the $2s^2 2p^3(^4S)4p \ ^{3,5}P$ and $2s^2 2p^3(^4S)5p \ ^{3,5}P$ levels is energetically allowed, but does not occur in practice.

V. CONCLUSION

We have analyzed the two-step Auger cascades following the resonant photoexcitation of the $1s^{-1}3p \ ^1P_1$ and $1s^{-1}4p \ ^1P_1$ core-excited levels in neon. Extensive MCDF calculations have been carried out to incorporate all ma-

ajor correlation contributions in the representation of the initial, intermediate and final states of the cascade. In addition, we have for the first time taken into account the important (single-electron) shake processes that are known to play an essential role in describing these Auger cascades. To this end, we applied the biorthonormal transformation to the atomic orbitals and the representation of the separately optimized atomic states. With this approach, we are able to simulate Auger electron spectra and to predict ion yields as well as shake probabilities that are in very good agreement with experiments. So-called conjugate shake processes to the $3d$ subshell are however found to be suppressed by several orders of magnitude compared to the dominating spectator and shake processes in the first step of the cascade. For the second step, we also found the (yet) unobserved weak decay channels $2s^0 2p^6 n\ell \rightarrow 2s^2 2p^4$ and $2s^0 2p^6 n\ell \rightarrow 2s^2 2p^3 n'\ell'$ which include a conjugate shake-down $2p \rightarrow 2s$.

In conclusion, our theoretical study clearly demonstrates that, apart from selected Auger lines, one can meanwhile simulate whole electron spectra or even (multiple) decay cascades with quite satisfying accuracy. This requires extensive computations with correlated wave functions, for which the MCDF method has been found versatile. While the autoionization of inner-shell excited neon atoms still refers to a rather simple system, we plan to extend these computations towards more complex atoms and/or Auger cascades. A careful theoretical analysis of such cascades may support also ongoing developments of new (magnetic-bottle) coincidence techniques as well as of time- and position-resolved detectors.

ACKNOWLEDGMENTS

We would like to thank Yusuke Tamenori for providing the experimental data from Ref. [8]. This research was funded by the German Federal Ministry of Education and Research (BMBF) under Contract No. 05K16SJA.

-
- [1] T. A. Carlson and M. O. Krause, *Phys. Rev. Lett.* **14**, 390 (1965).
 - [2] W. Eberhardt, G. Kalkoffen, and C. Kunz, *Phys. Rev. Lett.* **41**, 156 (1978).
 - [3] H. Aksela, S. Aksela, J. Tulkki, T. Åberg, G. M. Bancroft, and K. H. Tan, *Phys. Rev. A* **39**, 3401 (1989).
 - [4] H. Aksela, S. Aksela, H. Pulkkinen, A. Kivimäki, and O.-P. Sairanen, *Phys. Scr.* **41**, 425 (1990).
 - [5] Y. Shimizu, H. Yoshida, K. Okada, Y. Muramatsu, N. Saito, H. Ohashi, Y. Tamenori, S. Fritzsche, N. M. Kabachnik, H. Tanaka, and K. Ueda, *J. Phys. B* **33**, L685 (2000).
 - [6] A. Kivimäki, S. Heinäsmäki, M. Jurvansuu, S. Alitalo, E. Nömmiste, H. Aksela, and S. Aksela, *J. Electron Spectrosc. Relat. Phenom.* **114–116**, 49 (2001).
 - [7] A. De Fanis, G. Prümper, U. Hergenahn, E. Kukk, T. Tanaka, M. Kitajima, H. Tanaka, S. Fritzsche, N. M. Kabachnik, and K. Ueda, *J. Phys. B* **38**, 2229 (2005).
 - [8] Y. Tamenori and I. H. Suzuki, *J. Phys. B* **47**, 145001 (2014).
 - [9] Y. Hikosaka, T. Kaneyasu, P. Lablanquie, F. Penent, E. Shigemasa, and K. Ito, *Phys. Rev. A* **92**, 033413 (2015).
 - [10] J. Viefhaus, A. N. Grum-Grzhimailo, N. M. Kabachnik, and U. Becker, *J. Electron Spectrosc. Relat. Phenom.* **141**, 121 (2004).
 - [11] S. Schippers, A. Borovik Jr., T. Buhr, J. Hellhund, K. Holste, A. L. D. Kilcoyne, S. Klumpp, M. Martins, A. Müller, S. Ricz, and S. Fritzsche, *J. Phys. B* **48**, 144003 (2015).
 - [12] A. Müller, A. Borovik, T. Buhr, J. Hellhund, K. Holste, A. L. D. Kilcoyne, S. Klumpp, M. Martins, S. Ricz, J. Viefhaus, and S. Schippers, *Phys. Rev. Lett.* **114**, 013002 (2015).

- [13] M. Ya. Amusia, I. S. Lee, and V. A. Kilin, *Phys. Rev. A* **45**, 4576 (1992).
- [14] F. Zhou, Y. Ma, and Y. Qu, *Phys. Rev. A* **93**, 060501(R) (2016).
- [15] H. Yoshida, K. Ueda, N. M. Kabachnik, Y. Shimizu, Y. Senba, Y. Tamenori, H. Ohashi, I. Koyano, I. H. Suzuki, R. Hentges, J. Viefhaus, and U. Becker, *J. Phys. B* **33**, 4343 (2000).
- [16] H. Yoshida, J. Sasaki, Y. Kawabe, Y. Senba, A. De Fanis, M. Oura, S. Fritzsche, I. P. Sazhina, N. M. Kabachnik, and K. Ueda, *J. Phys. B* **38**, 465 (2005).
- [17] M. Kitajima, H. Yoshida, A. De Fanis, G. Prümper, U. Hergenhahn, E. Kukk, T. Tanaka, K. Nakagawa, H. Tanaka, S. Fritzsche, I. P. Sazhina, N. M. Kabachnik, and K. Ueda, *J. Phys. B* **39**, 1299 (2006).
- [18] J. Andersson, R. Beerwerth, P. Linusson, J. H. D. Eland, V. Zhaunerchyk, S. Fritzsche, and R. Feifel, *Phys. Rev. A* **92**, 023414 (2015).
- [19] S. Schippers, R. Beerwerth, L. Abrok, S. Bari, T. Buhr, M. Martins, S. Ricz, J. Viefhaus, S. Fritzsche, and A. Müller, *Phys. Rev. A* **94**, 041401(R) (2016).
- [20] F. Da Pieve, L. Avaldi, R. Camilloni, M. Coreno, G. Turri, A. Ruocco, S. Fritzsche, N. M. Kabachnik, and G. Stefani, *J. Phys. B* **38**, 3619 (2005).
- [21] M. Kato, Y. Morishita, M. Oura, H. Yamaoka, Y. Tamenori, K. Okada, T. Matsudo, T. Gejo, I. H. Suzuki, and N. Saito, *AIP Conf. Proc.* **879**, 1121 (2007).
- [22] T. Åberg and G. Howat, in *Corpuscles and Radiation in Matter I*, Encyclopedia of Physics, Vol. 31, edited by S. Flügge and W. Mehlhorn (Springer-Verlag, 1982) pp. 469–619.
- [23] S. Fritzsche, *Comput. Phys. Commun.* **183**, 1525 (2012).
- [24] S. Fritzsche, B. Fricke, and W.-D. Sepp, *Phys. Rev. A* **45**, 1465 (1992).
- [25] J. Olsen, M. R. Godefroid, P. Jönsson, P. Å. Malmqvist, and C. Froese Fischer, *Phys. Rev. E* **52**, 4499 (1995).
- [26] P. Jönsson, X. He, C. Froese Fischer, and I. P. Grant, *Comput. Phys. Commun.* **177**, 597 (2007).
- [27] A. Kramida, Yu. Ralchenko, J. Reader, and NIST ASD Team, “NIST Atomic Spectra Database (version 5.4),” (2016), <http://physics.nist.gov/asd>.
- [28] K. Ueda, M. Kitajima, A. De Fanis, Y. Tamenori, H. Yamaoka, H. Shindo, T. Furuta, T. Tanaka, H. Tanaka, H. Yoshida, R. Sankari, S. Aksela, S. Fritzsche, and N. M. Kabachnik, *Phys. Rev. Lett.* **90**, 153005 (2003).
- [29] D. V. Morgan, M. Sagurton, and R. J. Bartlett, *Phys. Rev. A* **55**, 1113 (1997).
- [30] U. Becker, O. Hemmers, B. Langer, I. Lee, A. Menzel, R. Wehlitz, and M. Ya. Amusia, *Phys. Rev. A* **47**, R767 (1993).